DETERMINATION OF GLOBAL SOLAR RADIATION

USING TEMPERATURE-BASED MODEL

FOR DIFFERENT CLIMATE CONDITIONS FOR LIMPOPO PROVINCE OF SOUTH AFRICA

A Dissertation Submitted to the Department of Physics

For the fulfilment of a M.Sc. Degree in Physics

By

MATHEBE SAMPIE MPHAGAHLA

(Student number: 11541988)

In the Faculty of Science, Engineering and Agriculture

At the University of Venda

Thohoyandou, Limpopo Province

South Africa

Supervisor: Dr. N.E. Maluta

Co-supervisor: Mrs T.S. Mulaudzi

YEAR 2021

DECLARATION

I, SAMPIE MPHAGAHLA MATHEBE, declare that this research is my original work and has not been submitted for any degree at any other university or institution. The thesis does not contain other persons' writing unless specifically acknowledged and referenced accordingly.

Signed (Student):  **Date: .27 May 2021.....**

ACKNOWLEDGEMENTS

Glory to God.

Special thanks to the following people who contributed so much to this study:

The late Prof. V. Sankaran, first supervisor, who shaped, guided and supported me in this journey, may his soul rest in peace.

Dr. N.E. Maluta, second supervisor and Dr. T.S. Mulaudzi co-supervisor, for their inspiration in this study is much appreciated.

The Department of Physics, the support and permission to further my study.

My wife, Eustacia Mathebe for her encouragement and support in this study, I will forever cherish that.

My children Chriselda, Chrishando and Chrisantha thanks for their loyal support.

ABSTRACT

The research mainly focused on the determination of global solar radiation using temperature-based model by Hargreaves and Samani for the Northern regions of Limpopo Province of South Africa. The daily maximum and minimum temperature data measured at the following six (6) stations were used: Ammondale, Mutale, Nwanedi, Roedtan, Sekgosese and Xikundu for the period 2008 – 2010.

The values of empirical coefficient K_r for the Inland stations of South Africa were computed and used as an input to the model. The observed and calculated global solar radiation data were compared on the basis of the statistical error tests that is mean bias error (*MBE*), the mean percentage error (*MPE*) and the root mean square error (*RMSE*).

Based on the statistical results the model was found suitable to estimate monthly average daily global solar radiation for the regions listed above and elsewhere with similar climatic conditions and areas where the radiation data is missing or unavailable. Hence, the study will also help to advance the state of knowledge of global solar radiation to the point where it has applications in the estimation of monthly average daily global solar radiation across.

Key words: Solar energy; Global solar radiation (*H*); Temperature based model; Extra-terrestrial solar radiation (H_0); K_r –Empirical constant.

LIST OF TABLES

TABLE PAGE

LIST OF FIGURE

FIGURE PAGE

Table of Contents

CHAPTER 1

1. INTRODUCTION

An energy system can be thought of as a network consisting of production from energy sources, storage, transmission, distribution, and consumption of energy. The most important types of energy in an energy system are found within the transportation, heating and electricity sectors. These sectors often rely on traditional fossil fuel-based energy sources such as coal, oil and gas. However, with the challenge of climate changes in the world, it is vital to replace fossil fuels with significant amounts of renewable energy technologies such as solar, hydro and wind power in the energy systems [1]. South Africa is a developing country and its economy is derived mainly from manufacturing and mining which are mostly energy-intensive industries. Even though it has some of the cheapest electricity supplies, South Africa's use of energy has not been particularly efficient. South Africa has one potential provider of electricity called Eskom. Recently, Eskom has admitted that electricity supply will be highly constrained for at least the next five years, due to the drastic deterioration of power stations and the depletion of coal reserves, and this is further impacted by the quality of coal which is available [1, 2].

Solar radiation has been identified as the largest renewable energy resource on Earth. The energy source is more evenly distributed in the Sunbelt of the World than wind or biomass, allowing for more site locations [3]. The maximum intensity of solar radiation at the earth's surface is about 1.2 kW/m^2 but it is encountered only near the equator on clear days at noon. Under these ideal conditions, the total energy received is approximately 6-8 kWh/m^2 per day [4]. Solar energy is not available continuously because of the day/night cycle and cloud cover. Its intensity varies according to the season, geographical location, and position of the collector [5]. Studies on solar radiation have become an important issue for renewable energy issues stemming from oil crises, global warming, and other environmental problems, thus increasing the need for reliable measurements of surface solar radiation [6]. Accordingly, solar radiation was monitored by measuring the sunshine duration with Campbell-Stokes recorders. An estimation of the global solar radiation is then obtained through different empirical

formulas like the well-known Angstrom–Prescott equation. Although pyranometers are nowadays available to directly measure the global solar radiation, the sunshine duration is still an essential climatological parameter that is still monitored in many meteorological stations to extend the historical time series [7, 8]. The cost of establishing a weather station and high maintenance cost still affects the developing countries like South Africa.

The current study aims to advance the state of knowledge of global solar radiation to the point where it has applications in the estimation of daily, monthly and yearly average global solar radiation. This would be done through the determination of global solar radiation for the Northern regions of Limpopo Province. The daily maximum and minimum temperature data measured at Ammondale, Mutale, Nwanedi, Roedtan, Sekgosese and Xikundu stations during the period (2008–2010) were used to calculate the daily, monthly and yearly average values of global solar radiation using the Hargreaves and Samani model [9].

1.1. SOLAR ENERGY

Although there is much controversy, contradiction, and skepticism surrounding the estimates and potential of various energy resources, there is a common consensus on the potential of the Sun amongst all world energy experts, that's the ultimate source of energy for all the life forms. It is also the originator of all other sources of energy that exist on the face of the Earth. The annual solar energy reaching the Earth's surface is estimated to be between 2.9-3.2 million exajoules (EJ) which is given by 1 EJ = 10^{18} J). Therefore, the energy from the Sun is nearly 7000 times the global energy consumption in a year [10]. The energy content of the total non-renewable energy resources is approximately 325,300 EJ (oil, 8 690 EJ; gas, 17 280 EJ; uranium, 114000 EJ; coal, 185 330 EJ) and of other major renewables is estimated at 1 960 EJ (hydro, 90 EJ; wind, 630 EJ; photosynthetic storage biomass, 1 260 EJ); a very small fraction of annual solar radiation.

The potential of solar energy varies geographically along with other factors. Nevertheless, even the lowest estimate of 1575 EJ/yr is more than three times the current global primary energy consumption. This disproves the myth that economic applications of solar energy should only be restricted to the sunniest regions. If the

annual average horizontal surface irradiance, of approximately 170 W/m^2, is integrated over 1 year, the resulting 5.4 GJ that is incident on 1 m^2 at ground level is approximately the energy that can be extracted from one barrel of oil, 200 kg of coal, or 140 m^3 of natural gas [11]. Solar power is one of the most promising source of renewable energy. It is more predictable than wind energy and less vulnerable to changes in seasonal weather patterns than hydropower. Whereas generation of power from hydro, wind and geothermal sources is limited to sites where these resources exist in enough quantities and can be harnessed, solar energy can produce power at the point of demand in both rural and urban areas [12]. The energy content of solar radiation can either be used directly or converted into other energy forms useful in our daily lives; light, heat, electricity, fuels and other applications by solar technologies. Some applications like photovoltaic and solar thermal collectors, are more popular others are less known, like solar detoxification or solar distillation. Nevertheless, each solar application has a significance of its own. It is these diverse ways in which solar energy can be used that make it an attractive and important option to power different energy systems in all countries of the world.

1.2. THE SOLAR RADIATION DATA

The Sun is a sphere of intensely hot gaseous matter with a diameter of 1.4 million kilometers, interior temperatures of 15 million degrees Kelvin and a pressure of 70 billion times higher than Earth's atmospheric pressure [12]. At such high temperature and pressure the Sun is a natural house of several fusion reactions (hydrogen atoms combining to form helium atoms as one of the most important element) that releases a tremendous amount of heat in the form of radiation. The sun has been producing energy at the rate of 3.9 x 10^{26} W for around five billion years and will continue to do so for several future more billion years [10, 11]. Radiation travels outward from the Sun at the speed of light (300,000 km/s). Given the Earth-Sun distance of 150 million kilometers, it takes 8 minutes for solar radiation to reach Earth's surface. The energy intercepted by the Earth over 1000 years is equal to the energy emitted by the Sun in just 14 seconds. Solar radiation spreads over a wide spectrum of wavelengths, from the 'short-wave' infrared to ultraviolet. The pattern of wavelength distribution is critically determined by the surface temperature of the Sun. The amount of solar radiant energy falling on a unit surface area per unit time is called irradiance [10]. An integral of

irradiance over any convenient stated period is called irradiation. An average extra-terrestrial irradiance or flux density at a mean Earth-Sun distance is known as the solar constant and has a currently accepted value of 1367 W/m^2 with an uncertainty of the order of 1 %. Due to the Earth's rotation in an asymmetric orbit about the Sun and the contents of its atmosphere, a large fraction of this energy does not reach the ground. Solar radiation data just outside of the Earth's atmosphere can be predicted with high precision, as it fundamentally depends on astronomical geometric parameters. It is the surface prediction that is more difficult owing to the atmospheric interactions, varying cloud cover and differing soil surfaces . Solar radiation plays a crucial role in affecting the Earth's weather processes. Earth-Sun geometry is also an important concept as it helps to determine seasonal irradiation which has a direct impact on buildings and solar system designs [12- 13]. The radiation received at the Earth's surface consists of direct and diffuse (scattered plus reflected) short-wavelength radiation and long-wavelength radiation from the sky and clouds, originating as thermal emission or by the reflection of thermal radiation from the ground. When the Sun’s rays hit the atmosphere, the portion of the light that is scattered comes to the Earth as diffuse irradiation.

Direct radiation, often called sunshine in layman terms, is the radiation that has not experienced scattering in the atmosphere, so that it is directionally fixed, coming from the disc of the Sun. In practice, this includes a certain amount of diffuse solar radiation. The sum of diffuse and direct irradiance is called global or total irradiance. The interception of solar radiation by arbitrary surfaces is a function of their solar geometry and a determinant of their microclimatic interaction, i.e. the energy exchange between the surface and the surroundings. To maximize the amount of solar radiation received on a surface, it must be tilted towards the Sun. Likewise, the orientation of the surface is very important. Both optimum tilt and orientation depend on the time of the year with the former additionally depending on the latitude [13]

1.3. SOLAR DATA: ITS USE AND SIGNIFICANCE

The basic need for knowledge of the quantity of radiation that can be received and transformed into useful energy at a given time or during a given time interval at a given geographical place or region, is important for solar energy technologies developers. The need for measuring and maintaining solar radiation data is important in developed and developing countries. Solar data recording began in 1957 and since then many meteorological stations across the globe have gathered considerable data on solar radiation [12]. Solar radiation measuring stations provide information on how much of the Sun's energy strikes a unit surface of an area at a location on the Earth during a certain period, over days, months and years. They are available in several forms. A typical database comprises global, direct and diffuse solar irradiance, duration of sunshine and complementary data like cloud cover, atmospheric pressure, turbidity, humidity, temperature and etc. There are several important aspects in the understanding and the use of solar data: geographic information of the site; whether the measurements are instantaneous (irradiance) or cumulative values (irradiation) over some time (usually hour or day), the time step and period of measurement, the parameters (e.g. global, diffuse or direct) being measured, the instruments used, the receiving surface orientation (usually horizontal, sometimes inclined at a fixed slope, or normal to the beam radiation) and if averaged, the period over which they are averaged (like, daily, monthly and yearly averages of radiation) [12]. For the development of any solar energy project, site-oriented and long-term solar radiation data are needed right from resource assessment to design the system for evaluation and optimization of its performance and short-term prediction of solar radiation for operational feasibility. Such data is extremely vital in several fields of applications such as:

(a) Illumination

Day lighting design concepts require knowledge of solar radiation incident on the walls, apertures and other external building surfaces. For some time the building industry has been in need of a comprehensive reference that describes new and innovative technologies for utilizing daylight in buildings and assesses the performance of these systems. This information is of particular benefit to building design practitioners, lighting engineers, product manufacturers, building owners and property managers.

Innovative day lighting systems are assessed according to their energy savings potential, visual characteristics and control of solar radiation [12-13].

(b) Architectural and energy-conscious building designs

Solar data is useful in determining optimum building configurations, orientations and air-conditioning systems to minimize the energy load. Likewise, heating and cooling systems can be sized in accordance with the effects of Sun's exposure through window orientations and sizes on the energy consumption of a building. Engineers and architects can use this information combined with desired levels of natural lighting and building aesthetics to formulate the final building design. Because energy costs are a significant expense in building ownership, an energy-efficient design can significantly reduce the life-cycle cost of a building [12].

(c) Agricultural research

Solar data helps in the study of crop growth models and evapotranspiration estimates in the design of irrigation systems. Efficient water management of crops requires accurate irrigation scheduling which in turn requires the accurate measurement of crop water requirement. Irrigation is applied to replenish depleted moisture for optimum plant growth. Reference evapotranspiration plays an important role in the determination of water requirements for crops and irrigation scheduling. Various models/approaches varying from empirical to physically base distributed are available for the estimation of reference evapotranspiration. Mathematical models are useful tools to estimate the evapotranspiration and water requirement of crops, which is essential information required to design or choose the best water management practices [12].

(d) Solar energy technologies

Space and water heating, thermal photovoltaic, detoxification process, etc. require solar data for their design and effectuation. A common factor in all such applications is the end-use product. Generally, it is a direct function of the amount of solar radiation received and the conversion efficiency [11, 12].

1.4. NEED FOR SOLAR RADIATION DATA MODELLING

In a period of rapidly growing deployment of solar energy systems, the acquisition of solar data is imperative. It allows assessment of a solar system's performance concerning the technicalities, local geography and energy demand. This in turn helps to assess the feasibility and practical value of the solar energy application. However, irradiance measurement-networks or meteorological stations do not always provide enough geographically time-site-specific irradiance coverage. Quite often, solar energy projects are not backed up by the long-term measured solar database required at the place of interest, mainly due to the capital and maintenance costs that measuring instruments incur. Consequently, they need to be estimated from alternative information available at the site or a nearby location. This is where solar radiation modelling plays an important role. Another scenario, pertinent to the present research topic is the common availability of global radiation at most of the sites world-wide, but no records on either diffuse or direct components [12]. The solar radiation data recorded at the meteorological stations generally is measured on a horizontal surface. However, most of the solar energy applications involve tilted surface for optimal performance. The irradiance falling on it cannot be calculated unless both direct and diffuse components of global irradiance are known.

The portion of total solar radiation that is diffuse is about 10% to 20% for clear skies and up to 100% for cloudy skies. In North-Western Europe, on average over the year, approximately 50% of the solar radiation is diffuse and 50% is direct . Both are useful for most solar thermal applications. While direct radiation can be focussed to generate very high temperatures, diffuse radiation provides most of the' daylighting' and hence, is vital to building industries. Diffuse radiation is also used in analyzing the energy balance of the atmosphere and in photo-biological processes. Despite their utility, both diffuse as well as direct irradiation are not measured as frequently as their global counterpart. This is a very common situation worldwide. In the UK alone, only 9 out of 84 meteorological stations recording hourly global irradiation, measure direct and diffuse irradiation [13]. This calls for a need to estimate diffuse radiation from more frequently measured radiation components and weather elements. Once diffuse radiation is estimated from global solar radiation, the direct component can be calculated as a difference of the two. The estimated radiation can thus not only serve

the locations lacking solar data but also provide to fill the gaps in the meteorological data even where it is measured.

In summary, fossil fuels are non-renewable and the amount of oil and gas resources are depleting, hence we have to prepare ourselves to use renewable energy resources. The South African government through its policies, implement various renewable energy projects to harness energy from the Sun. Hence detailed information about the renewable energy potential is very important. For this purpose, a suitable model for the various climatic regions of South Africa need to be studied to estimate the global solar radiation as accurately as possible. The current study was focused primarily on the determination of global solar radiation using the Hargreaves and Samani temperature-based model for the Northern regions of Limpopo province, South Africa. The maximum and minimum daily temperature data for the following six (6) stations were used: Ammondale, Mutale, Nwanedi, Roedtan, Sekgose, and Xikundu for the period 2008 to 2010. The results from this study will pave the way to use a low-cost model, using the temperature based model, to determine solar radiation information in the Northern region of South Africa and assist the renewable energy technologists to install suitable systems to harness the renewable energy potential.

The specific objectives of the study were as follows:

- To analyze the global solar radiation, temperature, and other meteorological data received from Agricultural Research Council (ARC) and South African Weather Services (SAWS) and hence classify them according to the different climatic conditions for the identified sites.
- To compute the values of extraterrestrial solar radiation H_0
- To compute global solar radiation (H) from the temperature-based models.
- To compare the values obtained through the model and study the applicability of the model on the given location and determine measurement uncertainties with statistical analysis.

AN OVERVIEW

In chapter two which is litereature review, will be focusing on solar radiation, factors that affect it, its measurements and different instrumentation used to measure solar radiation. Chapter three will look at the methodology, study area, models used, extraterrestrial solar radiation and statistical analysis, while in chapter four will focus on the results and discussions, which will be based in the, literature review, temperature, extraterrestrial solar radiation, empirical constant, estimation of global solar radiation, the summary of the results and conclusion.

CHAPTER 2

2. LITERATURE REVIEW

2.1 SOLAR RADIATION

In this chapter we will be focusing on solar radiation, factors that affect it, its measurements and different instrumentation used to measure solar radiation.

Solar radiation is defined as the direct form of the abundant permanent solar energy resource which is available on earth, because of the nuclear fusion in the Sun. The surface of the Earth receives roughly one hundred thousand of this renewable energy of solar power at the Earth's surface at every moment [9]. Solar radiation and sunshine duration are the two most important variables in the energy budget of the Earth. Together, they play a useful role in the performance evaluation of renewable energy systems and many other applications like health, agriculture, and construction. The global solar radiation (*H*) is the sum of direct, diffuse, and reflected solar radiation [11 - 13].

Solar radiation is the basis for all life on Earth. Autotrophs, organisms that produce their food from the Sun (mainly plants), use solar energy along with carbon dioxide and water to produce simple sugars in a process called photosynthesis. Heterotrophs, organisms that eat other organisms (like animals and fungi), depend on autotrophs to form the bottom level of the food chain. Heterotrophs couldn't exist without autotrophs, and autotrophs couldn't exist without the Sun, so life as we know it depends on electromagnetic radiation [10]

2.1.1 Global solar radiation

Global solar radiation (*H*) is the energy transferred from the Sun in the form of radiant that reaches the atmosphere in the form of shortwave electromagnetic radiation and is absorbed by the surface of the Earth, causing the Earth to warm up. The warm Earth's surface emits a part of the absorbed energy in the form of longwave radiation to heat the surrounding air. This air is not directly heated by solar radiation but is heated by contact with the hot surface of the Earth. In such an operation, there is a phase lag between the solar radiation and temperature cycles [11].

About 99 percent of global solar radiation has wavelengths between 300 and 3000 nm. This includes ultraviolet (300-400 nm), visible (400-700 nm), and infrared (700-3000 nm) radiation. Direct solar radiation passes directly through the atmosphere to the Earth's surface, diffuse solar radiation is scattered in the atmosphere, and reflected solar radiation reaches a surface and is reflected to adjacent surfaces.

The visible portion of the solar radiation spectrum provides energy for photosynthesis, which is the primary gateway for inorganic carbon to become organic and support life on the Earth. Infrared light heats the ground and maintains an ideal environment for life. Global solar radiation drives the global water cycle and weather patterns [11]. In fact about half of the solar radiation absorbed by the Earth's surface is consumed by evapotranspiration on a global scale. Solar radiation is also used to generate electricity. Measuring global solar radiation can be accomplished with pyranometers and pyroheliometers.

2.1.2 Direct solar radiation

Direct radiation can also be called “beam radiation”. It is used to describe solar radiation travelling on a straight line from the Sun down to the Earth’s surface. Direct radiation has a definite direction. The reason why shadows are only produced when direct radiation is blocked is that, when the radiation is direct, the rays are all travelling in the same direction hence they can all be blocked at once by an object. Direct radiation is roughly 85% of the total insolation on striking the ground, this occurs when the sky is clear and the Sun is very high in the sky. In sunny regions and during summers, direct radiation accounts for about 70-80% of the total radiation present. In solar plants, solar tracking is implemented to absorb most of the direct radiation. If solar tracking system is not installed the valuable direct radiation would go un-captured [11].

2.1.3 Diffuse solar radiation

Diffuse radiation describes the sunlight that has been scattered by molecules and particles in the atmosphere but that has still made it down to the Earth’s surface. It goes in any direction, there is no specific direction. When the Sun is lower in the sky, the percentage of diffuse radiation goes up until it reaches 40% as the Sun is above

the horizon. The percentage of diffuse radiation is also increased by atmosphere conditions like clouds and pollution. On an extremely overcast day, almost 100% of the solar radiation is diffuse radiation. The larger the percentage of diffuse radiation, the less the total insolation [11].

Diffuse radiation in the sky is much greater in higher latitude, cloudier places than in lower latitudes and sunnier places. The percentage of the total radiation that is diffuse radiation is mostly higher in the winter than the summer in these higher latitudes and cloudier regions. As pollution increases the amount of diffuse radiation rises. In hilly regions and during winters, the percentage of diffuse radiation goes up. The maximum amount of diffuse radiation is captured by the solar panels when they are kept horizontally. This means, in the case of solar panels which are at an angle to track most of the direct radiation, the amount of diffused radiation captured by the panels will go down. The larger the angle which solar panels make with the ground, the lesser would be the quantity of diffuse radiation captured by the panels [12].

2.1.4 Reflected solar radiation

Reflected radiation describes sunlight that has been reflected off the non-atmospheric entities like the ground. Asphalt reflects about 4% of the light incident on it and the lawn about 25%. Solar panels tend to be tilted away from where the reflected light is faced and radiation merely accounts for a suitable part of the sunlight striking their surface. An exception is in very snowy conditions which can sometimes cause the percentage of reflected radiation to be quite high [12]. The reflected radiation is the component of radiation that is reflected from surfaces beside air particles. Radiation reflected from hills, trees, houses and water bodies account for reflected radiation. Reflected radiation generally accounts for a small percent of the global radiation but can contribute as much as 15% in snowy regions [12].

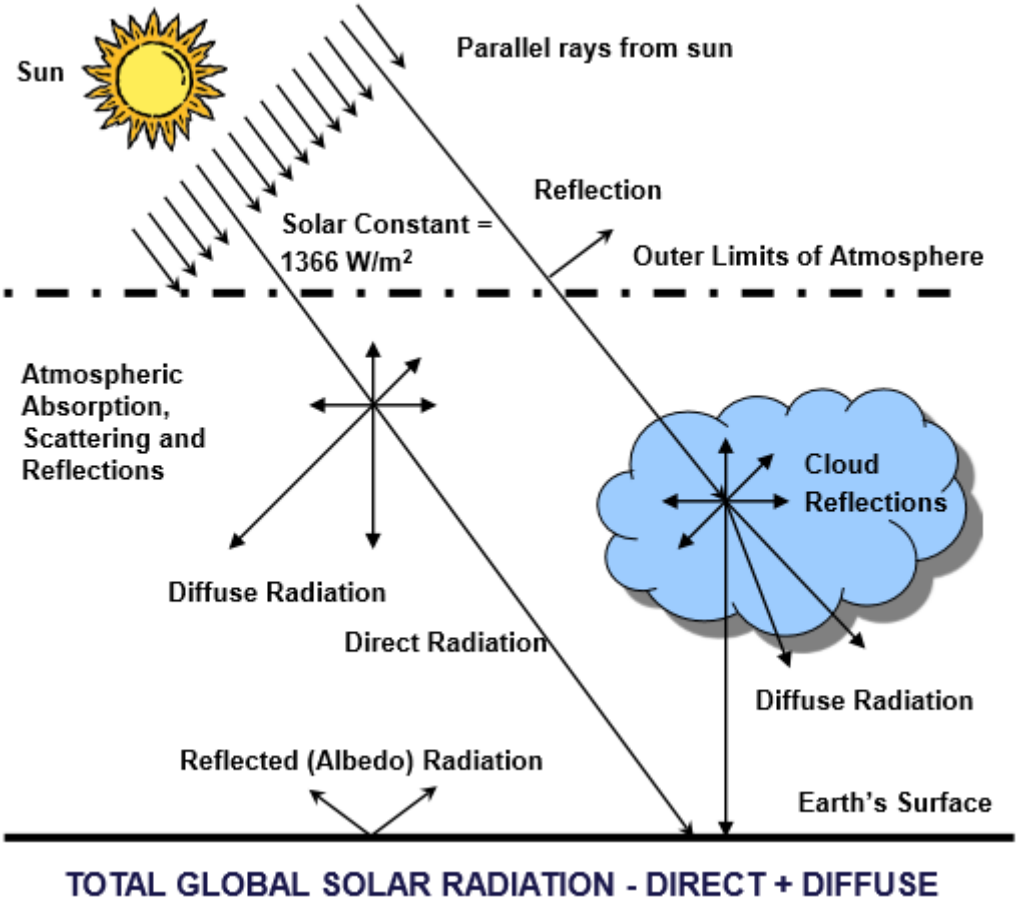

Figure 2.1: The total global solar radiation [12].

Figure 2.1 shows how solar radiation reaches the surface of the Earth. If the amounts of radiation energy absorbed, reflected and transmitted when radiation strikes a surface are measured in percentage of the total energy in the incident electromagnetic waves the total energy is divided into three groups. Absorptivity (α), reflectivity (ρ) and transmissivity (t). Absorption is the fraction of radiation absorbed by a surface, reflectivity is the fraction reflected by the surface and transmissivity is the fraction transmitted by the same surface.

Reflectivity deviates from the other properties from the fact that it is bidirectional in nature. In other words, this property depends on the direction of the incident of radiation as well as the direction of the reflection [12]. Therefore, the reflected rays of a radiation spectrum incident on a real surface in a specified direction forms an irregular shape that is not easily predictable. In practice, surfaces are assumed to reflect in a perfectly specular or dfuse manner. In a specular reflection, the angles of reflection and incidence are equal. In diffuse reflection, radiation is reflected equally in

all directions. Reflection from smooth and polished surfaces can be assumed to be the specular reflection, whereas reflection from rough surfaces approximates diffuse reflection [12]. In radiation analysis, a surface is defined as smooth if the height of the surface roughness is much smaller relative to the wavelength of the incident radiation.

2.2 FACTORS THAT AFFECT SOLAR RADIATION

The following are the factors that affect solar radiation [3,14,15,16]:

- Geographic location: This refers to a position on Earth and is defined by two coordinates, longitude and latitude. These two coordinates can be used to give specific locations independent of an outside reference point.
- Time of day: This refers to a loosely specified period of time, minutes or hours in duration especially daytime or point in time.
- Seasons: This refers to a period of the year that is distinguished by special climatic conditions.
- Local landscape: This refers to the visible features of an area of land, its landforms and how they integrate with natural or man-made features in a particular location in a country and this includes the physical elements of geophysically defined landforms such as (ice-capped) mountains, hills, water bodies such as rivers, lakes, ponds and many more.
- Local climatic conditions: This refers to the description of the long-term pattern of weather in a particular area.

As shown in Figure 2.1, the distribution of solar radiation is affected by various factors.

2.2.1 Geographic location

It is known that the Earth is round, the Sun strikes the surface at different angles, which range from 0° (just above the horizon) to 90° (directly overhead). When the Sun's rays are vertical, the Earth's surface receives all the energy possible. The more slanted the Sun's rays are, the longer they travel through the atmosphere becoming more scattered and diffused. Consequent to the Earth roundness results in frigid polar regions that never receive a high Sun. Because of the tilted axis of rotation, these areas receive no Sun at all during some part of the year [13].

Local geographical features, such as mountains, oceans, and large lakes, influence the formation of clouds, therefore, the amount of solar radiation received from these areas may be different from that received by the adjacent land areas. For example, mountains may receive less solar radiation than adjacent foothills and plains located a short distance away. Winds blowing against mountains force some of the air to rise, and clouds form the moisture in the air as it cools. Coastlines may also receive a different amount of solar radiation than areas further inland. Where the changes in geography are less pronounced, such as in the high veld the amount of solar radiation is less variable [14].

2.2.2 Time of day

The Earth revolves around the Sun in an elliptical orbit and is closer to the Sun during Autumn. When the Sun is nearer the Earth, the Earth's surface receives a little more solar energy . Generally, more solar radiation is present during midday than during either the early morning or late afternoon. During midday, the Sun is positioned high in the sky and the path of the Sun's rays through the Earth's atmosphere is shortened. Consequently, less solar radiation is scattered or absorbed and more solar radiation reaches the Earth's surface. In the Northern Hemisphere, South-facing collectors also receive more solar radiation during midday because the Sun's rays are nearly perpendicular to the collector surface [13,14].

Tracking collectors can increase the amount of solar radiation received by tracking the Sun and keeping its rays perpendicular to the collector throughout the day. In the Southern Hemisphere, we also expect more solar radiation during the Summer than during the Winter because there are more daylight hours. This is more pronounced at higher latitudes [15].

2.2.3 Seasons

The 23.5° tilt in the Earth's axis of rotation is a more significant factor in determining the amount of sunlight striking the Earth at a particular location. The Earth is nearer the Sun when it is Summer in the Southern hemisphere and Winter in the Northern hemisphere [13]. However, the presence of vast oceans moderates the hotter Summers and colder Winters as one would expect to see the result of this difference.

Tilting results in longer days in the Northern hemisphere from the Spring (vernal) equinox to the fall (Autumnal) equinox and longer days in the Southern hemisphere during the other 6 months. Days and nights are both exactly 12 hours for both Southern and Northern hemisphere.

At the equator the daily period of daylight is the same day after day. The changing path of the Sun through the sky produces over the year a cyclical variation in the amounts of solar radiation received that exhibit maxima near the equinoxes and minima near the solstices. The relatively little variation in the amounts of solar energy received over the year produces seasons quite different from those experienced at higher latitudes [13].

Away from the tropics, the variation in the amount of solar radiation received over the year increases as latitude increases. The amount of sunlight received exhibit one minimum and one maximum in their annual swings. The poles have the greatest range since the Sun is in their skies continuously for six months and then below the horizon for the other half year. Generally, the variations in solar radiation received at the surface over the year at higher latitudes create greater seasonal differences whilst the receipt of solar energy is the major cause of seasonal swings of weather and climate at the middle and high latitudes [14].

2.2.4 Local landscape

Almost all human activities such as agriculture, forestry, building design, and land management ultimately depend upon insolation. At a global scale, the latitudinal gradients of insolation, caused by the geometry of the Earth's rotation and revolution about the Sun are well known. At the landscape scale, the topography is the major factor modifying the distribution of insolation. Variability in elevation, surface orientation, thus slope, aspect and shadows cast by topographic features create strong local gradients of insolation[16].

Accurate insolation maps at landscape scales are desired for many applications. Although there are thousands of solar radiation monitoring locations throughout the World, for most geographical areas accurate insolation data are not available. Simple interpolation and extrapolation of point-specific measurements to areas are generally not meaningful because most locations are affected by strong local variations.

Accurate maps of insolation would require a dense collection station network, which is not feasible because of the high cost [16]. Network densification is attracting increasing attention recently due to its ability to improve network capacity by spatial reuse and relieve congestion by offloading. However, excessive densification and aggressive offloading can also cause the degradation of network performance due to problems of interference and load [16].

2.2.5 Local climatic conditions (Weather)

The rotation of the Earth is also responsible for hourly variations in sunlight. In the early morning and late afternoon the Sun is low in the sky. Its rays travel further through the atmosphere than at noon when the Sun is at its highest point. On a clear day, the greatest amount of solar energy that reaches a solar collector is around solar noon [13]. Although the climate system is in balance, the balance of the climatic system is dynamically needed as an ever-changing system. The system is constantly adjusting to forcing perturbatios and, as it adjusts, the climate alters. A change in any part of the climate system will have much wider consequences as the initial effect cascades through the coupled components of the system.

As the effect is transferred from one sub-component of the system to another, it will be modified in character or scale [16]. The amount of incoming solar radiation is balanced by the amount of outgoing terrestrial radiation so that the Earth does not continue to heat up or cool down indefinitely. The Earth's climate is said to exist in equilibrium. When the climate system responds to radioactive forces, this equilibrium is temporarily upset and a discrepancy between incoming and outgoing radiation exists. In an attempt to restore equilibrium, the global climate subsequently alters by either heating up or cooling down depending on the direction of initial forces [16].

2.3 MEASUREMENTS OF SOLAR RADIATION

Solar radiation has been a subject of interest throughout history. The earliest investigation of the Sun and its properties was, most probably, that of Galileo Galilei (1611) following the famous invention of the telescope [17]. Since then, much of the seventeenth century, some of the eighteenth century and whole of the nineteenth

century saw various discoveries and explanation of now well-known concepts such as: the spectral character of light, law of refraction, phenomenon of diffraction, light's speed, wave theory of light, polarization of light, electromagnetic theory of radiation, the colour of sunlight sky, radiation scattering, polarization's wavelength dependence, solar radiation absorption by water vapour, etc [17].

Global and diffuse solar radiation are measured by a pyranometer. For the diffuse, a pyranometer must have a shadow. Direct solar radiation is measured using a pyrheliometer. The pyrheliometer measures radiation at normal incidence [17].

2.3.1 Pyranometer

Figure 2.2: Pyranometer [18]

A pyranometer illustrated in Figure 2.2 is a type of actinometer which measures solar irradiance and solar radiation flux density in the desired location. The solar radiation spectrum extends approximately between 300 and 2800 nm. The pyranometer only requires a flat spectral sensitivity to help cover this spectrum [18]. There are different types of pyranometers that are available from manufacturers such as Kipp Zonnen, Hukseflux, EKO, etc. [18]. So to make a measurement of irradiance, it is required by definition that the response to "beam" radiation varies with the cosine of the angle of incidence. This ensures a full response when the solar radiation hits the sensor perpendicularly (normal to the surface, Sun at zenith, 0° angle of incidence), zero response when the Sun is at the horizon (90°C angle of incidence, 90°C zenith angle), and 0.5 at a 60°C angle of incidence. It follows that a pyranometer should have a so-

called "directional response" or "cosine response" that is as close as possible to the ideal cosine characteristic [18].

The light sensitivity known as 'spectral response', depends on the type of pyranometer. The figure here above shows the spectral responses of the three types of pyranometer in relation to the solar radiation spectrum. The solar radiation spectrum represents the spectrum of sunlight that reaches the Earth's surface at sea level, at midday with A.M. (air-mass) =1.5. The latitude and altitude influence this spectrum. The spectrum is influenced also by aerosol and pollution [19].

2.3.1.1 Thermopile pyranometer

A thermopile pyranometer is a sensor based on thermopiles designed to measure the broadband of the solar radiation flux density from a 180°C field of view angle. A thermopile pyranometer thus usually measures 300 to 2800 nm with a largely flat spectral sensitivity. The first generation of thermopile pyranometers had the active part of the sensor equally divided in black and white sectors [19 - 20].The thermopile pyranometer calculate the Irradiation from the differential measured between the temperature of the black sectors, exposed to the Sun and the temperature of the white sectors, sectors not exposed to the Sun or more accurately in the shade. In all thermopile technology, irradiation is proportional to the difference between the temperature of the Sun exposed area and the temperature of the shadow area [21].

Figure 2.3: Thermopile pyranometer [19]

A thermopile as shown in Figure 2.3 is used within the instrument as the sensor, and the thermal gradients are measured across hot and cold areas (black and white). The radiation intensity is proportional to the temperature differences between the two sensing areas. Accuracy depends upon the sensitivity of the material used in the sensors, the response time and the distortion characteristics of the material constituting the dome (if present) covering the sensors [19].

2.3.1.2 Photodiode-based pyranometer

The photodiode-based pyranometer is also known as a silicon pyranometer. In the ISO 9060, a photodiode-based pyranometer can detect the portion of the solar spectrum between 400 nm and 900 nm, with the most performant detecting between 350 nm and 1100 nm. The photodiode converts the aforementioned solar spectrum frequencies into current at high speed, the conversion is influenced by the temperature with a rise in current produced by the rise in temperature (about 0, 1% °C) [20].

2.3.1.3 Photovoltaic pyranometer

Figure 2.4: Photovoltaic pyranometer [20]

Built in the 2000s concurrently with the spread of photovoltaic systems, the photovoltaic pyranometer illustrated in Figure 2.4 is a derivation of the photodiode pyranometer, and it answered the need for a single reference photovoltaic cell when

measuring the power of cell and photovoltaic modules. Specifically, each cell and module is tested through flash tests by their respective manufacturers, and thermopile pyranometers do not possess the adequate speed of response nor the same spectral response of a cell. This would create an obvious mismatch when measuring power, which would need to be quantified. In technical documents, this pyranometer is also known as a "reference PV cell", and "irradiance sensor", "solar meter", and “solar sensor”, in works more recent than the ISO 9060 [21].

The active part of the sensor is composed of a photovoltaic cell working in a near short-circuit condition. As such, the generated current is directly proportionate to the solar radiation hitting the cell in a range between 350 nm and 1150 nm. When it is struck by a luminous radiation in the mentioned range, it produces current as a consequence of the photovoltaic effect; its sensitivity is not flat, but it is the same as that of silicon photovoltaic cell [21].

2.3.2 Pyrheliometer

Figure 2.5: Pyrheliometer [21]

A pyrheliometer shown in Figure 2.5 is a broadband instrument that measures the direct (or beam) component of solar radiation at normal incidence and hence the instrument is always aimed directly at the Sun, through a tracking mechanism that continuously follows the Sun. It is sensitive to wavelengths in the band from 280 to 3000 nm [21]. Pyrheliometer measurement specifications are subject to International

Organization for Standardization (ISO) and World Meteorological Organization (WMO) standards.

Comparisons between pyrheliometers for intercalibration are carried out regularly to measure the amount of solar energy received. The aim of the International Pyrheliometer Comparisons, which take place every 5 years at the World Radiation Centre in Davos, is to ensure the world-wide transfer of the World Radiometric Reference. During this event, all participants bring their instruments, solar-tracking and data acquisition systems to Davos to conduct simultaneous solar radiation measurements with the World Standard Group. There are different types of pyrheliometers that are available from manufacturers such as Hukse flux, EKO, etc. [21].

2.3.2.1 SHP1

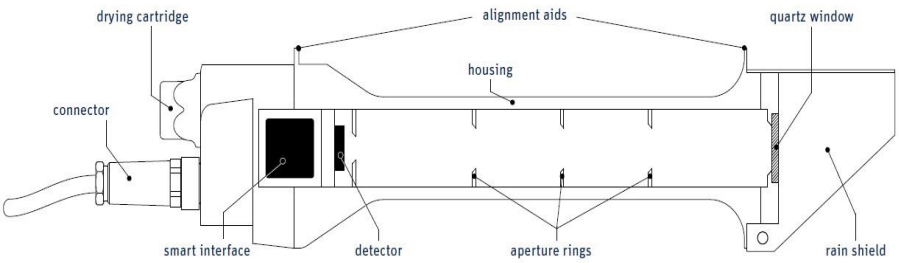

Figure 2.6: SHP1 [22]

SHP1 illustrated in Figure 2.6 is a pyrheliometer device well equipped with an interface having both digitized RS 485 Modbus (it defines the electrical and characteristics of drivers and receivers) and an intensified analogue output. This pyrheliometer offers a smart interface and is an advancement of the CPH 1 version. Moreover, the SHP1 also has a response period below 2 seconds. The individually measure temperature correction varies from negative 40°C to positive 70°C. Combining the SHP 1 sensor technology with smart interface advantages makes the SHP1 the best commercially available pyrheliometer [20]. The smart interface not only offers versatile outputs, the integrated temperature sensor and digital polynomial functions also provide individual correction for the temperature sensitivity mentioned above.

The increased response time and the standard output help interchange instruments for recalibration. SHP1 pyrheliometers have very low power consumption so that

internal heating does not affect the detector performance. SHP1 pyrheliometer is available in two versions, one has an analogue output of 0-1V the other is 4-20mA. Both have a 2-wire RS-485 interface with Modbus (RTU) protocol. The analogue outputs enable easy connection to virtually any data logger without the need for sensitive mV inputs [22].

2.3.2.2 CHP1

Figure 2.7: CHP1 [23]

CHP1 as shown in Figure 2.7 is a type of pyrheliometer which completely complies with the latest standards set by International Standardization Organization (ISO) and World Meteorological Organization (WMO) regarding the criteria for First Class Normal Incidence Pyrheliometer. Each pyrheliometer is checked for manufacturing and supply standards with a traceable checking certificate issued by the World Radiometric Reference (WRD) [23].

To monitor direct normal irradiance, a CHP1 Pyrheliometer is mounted to a user-supplied Sun tracker such as Kipp & Zonen's Solys2. The CHP1 pyrheliometer measures the direct-beam solar irradiance with a field of view limited to 5 degrees.

The limited field of view requires the CHP1 to be continuously pointed toward the Sun. The Solys2 Sun Tracker rotates on two axes and uses a GPS receiver to keep the CHP1 aimed at the Sun throughout the day [23].

2.4 EMPIRICAL MODELS FOR ESTIMATING GLOBAL SOLAR RADIATION

Through the centuries, scientists have found innovative ways to harness the power of the Sun. Increasing the conversion of solar power into electricity is highly present on the political agenda in many countries, amid the push to find domestic energy sources that are less polluting than fossil fuels. Solar energy technologies use the Sun's energy and light to provide heat, light, hot water, electricity, and even cooling, for houses, businesses and industries [24].

Solar radiation is the fundamental renewable energy source that sustains the biosphere and drives its self-organization. Reliable solar radiation data sets are essential to the work of energy planners, engineers and agricultural scientists. Determination of the solar energy capacity of a region requires that extensive radiation measurements of high quality be made at a large number of stations covering the major climatic zones of the region. Several empirical models have been developed to calculate the solar radiation using various parameters. These parameters include extraterrestrial radiation, sunshine hours, relative humidity, temperature, soil temperature, number of rainy days, altitude, latitude, total perceptible water, cloudiness and evaporation [25 - 26].

2.4.1 Temperature-based models

Some of the temperature-based models use maximum and minimum air temperature to estimate atmospheric transmissivity [26]. These models assume that maximum temperature will decrease with reduced transmissivity, whilst minimum temperature will increase due to the cloud emissivity. Clear skies will increase maximum temperature due to higher short wave radiation, and minimum temperature will decrease due to higher transmissivity so the difference between daily maximum and minimum air temperature becomes an indicator of cloudiness. Although cloud cover

decreases maximum and minimum air temperature, clearly, many others factors, such as wind speed, air-vapor, precipitation, frontal weather systems, evaporation, etc., also affect temperature levels. For this reason, models applied on daily time steps have substantially greater uncertainty and prediction error. Methods are recommended to use with five-day or longer time steps [27].

2.4.1.1 Hargreaves and Samani model

Hargreaves and Samani were the first to suggest that incident radiation could be evaluated from the difference between daily maximum and daily minimum temperature. The equation introduced by Hargreaves and Samani is given as [26]:

$$H = K_r H_o \sqrt{T_{max} - T_{min}}, \quad (1)$$

where, H (MJ/m^{2}day) is the estimated global solar radiation, H_o (MJ/m^{2}day) is the extraterrestrial solar radiation, T_{max} (°C) is the maximum daily temperature, T_{min} (°C) is the minimum daily temperature and K_r (°C$^{-0.5}$) is an empirical coefficient. Hargreaves recommended to use K_r = 0.16 for interior regions (inland) and K_r = 0.19 for coastal regions. The equation is based on the assumption that the difference between daily maximum and minimum temperatures provides a general indication of cloudiness [26].

2.4.1.2 Annandale model

The modified Hargreaves–Samani model developed by Annandale is given as [27]:

$$H = K_r H_o (1 + 2.7 * 10^{-5} Z) \sqrt{T_{max} - T_{min}}, \quad (2)$$

where K_r is an empirical coefficient and for the current study is 0.16 for the interior region and 0.19 for coastal region Z is the altitude. The coefficient must be derived at a site where data measurements are available [27]. It is known and understood by many scientists that solar energy is one of the potential ways for man to escape the current tight spot regarding fossil fuels [28]. But, only a tiny fraction of available solar energy is harnessed by renewable energy technologies today; if it were possible to funnel more of that raw energy into electricity that could be used for homes, businesses, and appliances, it would represent a solution to one of mankind's biggest problems. Unsurprisingly, many scientists have consequently dedicated a great deal of research to the potential use of solar energy. Sunlight warms us (meaning that for

our body to function well Vitamin D is needed), feeds us (plants make their own food during the process, photosynthesis, human and animals are the beneficiaries), and essentially lights up the lives of all creatures on Earth even for modern, less spiritual cultures, this is something to be appreciated [29].

2.4.1.3 Chen model

Chen represented their model as follows [27]:

$$H = H_0 \times 0.264341 \ln(T_{max} - T_{min}) - 0.155612 \quad (3)$$

2.4.1.4 Bristow and Campbell model

Bristol and Campel develop the equation to estimate the global solar radiation in a different form in which H is an exponential function of ΔT and is given as [27,29]:

$$H = H_o \times a[1 - exp(-b\Delta T^c)] \quad (4)$$

where $\Delta T = T_{max} - T_{min}$

2.4.1.5 Clemence model

Clemence developed a model given by the equation [29]:

$$H = H_0(1.233 \times \Delta T + 10.593 \times T_{max} - 0.713 \times T_{max}\Delta T + 16.548 \times 0.0418) \quad (5)$$

The clemence model was developed for the Southren Africa region and it is one of the best model to be used in Africa as a continent.

The contributions made by solar energy are enormous, and its future potential as an alternative power source for modern life makes the Sun one of the most important natural resources available today [30]. Early in the 7th Century BC humans were harnessing the Sun for solar energy. The Greeks and Romans were the first to use concentrated solar rays to ignite fires, illuminate their buildings, and even as military weapons [31]. As early as the 1st Century AD, humans were taking advantage of solar energy by building homes with South-facing windows to provide heat. In 1767, Horace

de Saussure created the world's first solar collector to cook food and became the first individual to create a device that actively took advantage of the Sun's rays [32].

In the 19th century progress was made towards the mechanical conversion of light into energy, with the discovery of the photovoltaic effect, the photoconductive nature of selenium, that when exposed to light generates an electric current. This principle is the foundation of today's solar panel technology [33]. In 1891, the first solar water heater was invented, which is an early predecessor to today's solar thermal technology. In 1954, Bell Laboratories patented the first solar photovoltaic technology capable of creating enough electricity to power electronic devices. It was only 4-11% efficient. The 1970s witnessed a significant reduction in the price of solar cells, with the cost falling from around $100 per watt to around $20 per watt [34,35].

2.5 SOME OTHER MODELS USED TO PREDICT GLOBAL SOLAR RADIATION.

In general, there are different empirical formula which are used to estimate global solar radiation. The current study only focuses on the temperature-based model to validate it for different climate conditions in the Limpopo province of S.A. sunshine hours, rainfall, humidity, cloud, etc, models are available in literature to estimate the global solar radiation. In 1988 McCaskill reported a model of estimation of solar radiation using rainfall only using Fourier series with incorporated rainy-day information as [36]

$$H = H_0 a(1 - \exp(-bD^C)) \quad , \tag{6}$$

where *a*, *b* and *c* are empirical coefficients, determined for a particular site from measured solar radiation data. *D* is the diurnal range of air temperature and is calculated as,

$$D = T_{max} - \frac{T_{\min(j)} + T_{min(j+1)}}{2}, \tag{7}$$

where T_{max} is the daily maximum temperature (°C), T_{min}(j) and T_{min}(j+1) the daily minimum temperature (°C) on the day and the next day, respectively. The underlying principle of this approach is to use the diurnal temperature range as an indicator of overcast conditions that would impact on the transmittance of radiation. Bristow and Campbell in 1984 included an adjustment for the measured *D* on the rainy days as the rainfall can be another manifestation of cloud cover [37]. However, we do not include

an adjustment as we use the method for estimating radiation in the case when rainfall data are not available.

The Hargreaves and Samani model was modified by Hargreaves [31] also Richardson equation (8) [37]. The modified equations by Hargreaves has modified the model to be equation (9) and Richardson modified it to equation (8) are given as [37]:

$$H = H_0 a(T_{max} - T_{min})^b, \quad (8)$$

$$H = H_0 a\sqrt{T_{max} - T_{min}} + b\ , \quad (9)$$

In another study, McCaskill related *H* to H_0 and rain-day information as [38]

$$H = \alpha H_0 + bR_{j-1} + cR_j + dR_{j+1}\ , \quad (10)$$

where α is the day of the year converted to radian, *R* the transformed rainfall data and the subscripts, j, j−1 and j+1 refer to current, previous and next days, and *b, c, d* are the regression coefficients. The transformation used to calculate R (rainfall) data was to encode rain-days: if P>0, R=1; P=0, R=0, where P is precipitation in (11). Estimation of solar radiation using both temperature and rainfall model was reported by McCaskill which uses the precipitation and the range of daily temperature as:

$$H = aH_0 D^b(1 + cP + dP^2), \quad (11)$$

where *a, b, c* and *d* are regression coefficients and *R* is as defined in Equation (10). The coefficient *a* is the atmospheric transmittance with no rainfall recorded on the day, the day before or the day after, while *b, c,* and *d* are the amounts of radiation reduction (MJ $m^{2)}$ when it rained on the day before, on the day and on the day after, respectively [39]. While P is the total precipitation (mm) on the day, D is defined as in equation (7). Richardson [37] developed equation (8) to include the effect of *P* as an additive formula:

$$H = H_0 a\sqrt{T_{max} - T_{min}} + bT_{max} + cP + dP^2 + e\ , \quad (9)$$

where *a, b, c*, *d*, *e* are the regression coefficients. By analysing various forms with both temperature and rainfall variables across Australia, they propose two equations in the form of [40]:

$$\frac{H}{H_0} = a\left(\frac{RH}{100}\right) + b\left((T_{max}-T_{min})\right)^{0.5} + c(T_{max} - T_{min}) + d\left(\frac{RH}{100}\right)\left((T_{max} - T_{min})\right)^{0.5} + e \quad (10)$$

$$\frac{H}{H_0} = a.\left[1 - exp(-\Delta T^b)\right] + c.RH\ , \quad (11)$$

where *a, b, c, d* and *e* are the empirical coefficients, and *RH* is the relative humidity. The expression for the three rainfall is consistent with McCaskill which was discovered in 1990 [40].

In equation (11), the coefficient *a* is the maximum clear sky atmospheric transmittance (ξ_{mx}) which is defined as the ratio of *H* to H_0 when *D* is very large. In equation (10), ξ_{mx} at the given site can be approximated whenever $g = 0.0$, $\xi_{mx} = a$; when $g \neq 0$, ξ_{mx} is a function of H_0. Hence, ξ_{mx} varies with season. When $g > 0$, ξ_{mx} is larger in winter than in summer; that is the atmospheric transmittance in winter at this site is higher than in summer [41]. When g < 0, the atmospheric transmittance in Winter at this site is less than in summer. Therefore, *g* accounts for the seasonal changes in atmospheric transmittance for the site. Three popular models used to measure global solar radiation using temperature minimum and maximum and other meteorological data are Genetic algorithm (GA), Statistical regression technique (SRT) and Artificial neural networks (ANN). There are different kinds of models used to predict global solar radiation data using temperature (maximum and minimum), humidity, cloud cover, sunshine hours, rainfall, wind speed or direction data. The most used Angstrom regression model relates monthly average daily radiation to a clear day radiation in a given location and average fraction of possible sunshine hours as [42]:

$$\frac{H}{H_0} = a + b * \frac{S}{S_0}\ , \quad (12)$$

where *H* is the monthly average daily global radiation, (H, MJ/m^2), H_0 is the monthly average extraterrestrial radiation, *a* and *b* are the regression coefficients, *S* is the actual measured sunshine duration, and S_0 is the maximum daily sunshine duration. Apart from the sunshine hours based model and temperature data based model to estimate the global solar radiation there are models that combines the sunshine hours and temperature data to compute the global solar radiation one of the model is defined in the form [35]:

$$\frac{H}{H_0} = a + b * \frac{\Delta T}{S_0}\ , \quad (13)$$

where *a* and *b* are Angstrom regression coefficients, ΔT is the difference between the daily maximum and minimum temperature and S_0 is the actual sunshine hours.

CHAPTER 3

In this chapter we will look at the methodology, study area, models used, extraterrestrial solar radiation and statistical analysis.

3. METHODOLOGY

3.1 THE STUDY AREA

South Africa is the southern most part of the African continent, its latitude is between 22^{o} and 35^{o} S and longitude 17^{o} and 33^{o} E. The surface area is 1,219,090 km^{2} and is split up into nine provinces, namely, Limpopo, Mpumalanga, Gauteng, North West, Free State, Kwazulu-Natal, Eastern Cape, Western Cape and Northern Cape. South Africa is a subtropical location and is famous for its sunshine [43]. The study focus on the Northern regions of the Limpopo province which can be observed in Figure 3.1. The Limpopo province is known to be a very hot area with higher temperatures throughout the year. The temperatures above 32^{o}C are very common in Summer and frequently exceed 35^{o}C. In September the temperatures may exceed the maximum of 43^{o}C [44]. For this study, six stations were considered, namely, Ammondale, Mutale, Nwanedi, Roedtan, Sekgosese and Xikundu. The geographical coordinates of the stations under study are listed in Table 1, where the lowest latitude is of Nwanedi at 24. 62472 ^{o}S and the highest latitude is in Roedtan at 22. 45404 ^{o}S and the lowest longitude is in radiation at 29.06759 ^{o}E and highest at Mutale with 30.52188^{o}E [45]

Figure 3.1: Map of Northern Regions of South Africa [45]

Limpopo province is situated at the North Eastern corner of South Africa and shares borders with Botswana, Zimbabwe and Mozambique. It forms the link between South Africa and countries further afield in Sub-Saharan Africa. It also offers a mosaic of exceptional scenic landscapes, a fascinating cultural heritage, an abundance of wildlife species and many nature-based tourism opportunities. Ammondale is influenced by the local steppe (a large area of flat unforested grassland) climate. There is little rainfall throughout the year. The average annual temperature in Ammondale is about 21.8 ^{o}C. the annual rainfall averages 600 mm.

The driest month is June, with 4 mm of rainfall. The greatest amount of precipitation occurs in February, with an average of 140 mm. The warmest month of the year is January, with an average temperature of about 26.0^{o}C [46, 47]. The lowest average temperatures in the year occur in July, where it is around 16.8^{o}C. The difference in precipitation between the driest month and the wettest month is 136 mm. The variation in temperatures throughout the year is 9.2^{o}C [46]. Mutale generally observes the Winter season during May, June and July. During this period, we normally expect lower actual sunshine hours than the other seasons.

But the actual sunshine hours are rather more during the years under investigation in Winter and this may be attributed to limited absolute clear sky days for that particular year [47]. In addition to that, it is always preferable to calibrate the measuring instruments on a regular basis in order to get a reliable set of data. Even when it is Winter the temperature remains high with minimum of 10^{o}C when it is extremely cold in the area and maximum temperature of 27^{o}C during Summer [48]. Nwanedi normally receives about 246 mm of rain per year, with most rainfall occurring mainly during Mid-Summer. It receives the lowest rainfall (0 mm) in June and the highest (55 mm) in January. The monthly distribution of average daily maximum temperatures shows that the average midday temperatures for Nwanedi range from 23.9^{o}C in July to 32.1^{o}C in January [49]. The region is at its coldest during July when the temperature drops to 7.6^{o}C on average during the night. Roedtan normally receives about 443 mm of rain per year, with most rainfall occurring during Summer. It receives the lowest rainfall (0 mm) in June and the highest (93 mm) in December. The monthly distribution of

average daily maximum temperatures shows that the average midday temperatures for Roedtan range from 21°C in June to 29°C in January. The region is at its coldest during June when the temperature drops to 4°C on average during the night [50, 51]. The climate here is considered to be a local steppe (a large area of flat unforested grassland) climate. In Roedtan, there is little rainfall throughout the year. The average temperature is 19.7°C. Precipitation here averages 532 mm. The driest month is July, with 3 mm of rain. With an average of 105 mm, the most precipitation falls in December, January is the warmest month of the year. The temperature in January averages to about 24.1°C [52]. June has the lowest average temperature of the year, about 12.9°C. There is a difference of 102 mm of precipitation between the driest and wettest months. During the year, the average temperatures vary by 11.2°C.

Sekgosese offers a relatively pleasant climate for most of the year, with almost all-year-round sunshine, it can get rather hot in the Summer months (October to March) averaging 27°C [53]. The Lowveld is less forgiving in the swelter of Summer afternoons, you will be surprised to find that later in the day the clouds grow heavy and expect thunderstorms. Winter is typically of the interior highveld plateau. A sunny season of chilly, early mornings, warm middays, dry afternoons, and cool to cold nights. In general, the weather of Sekgosese will greet you with a hospitable display of sunshine and reserve [54].

Table 3.1: Location of the selected meteorological stations

Station	Latitude (° S)	Longitude (° E)	Altitude (m)	Climate condition
Ammondale	- 23, 72619	29.59517	719	Temperate interior
Mutale	- 22, 73461	30, 52188	329	Hot interior
Nwanedi	- 22, 45404	30.50259	429	Hot interior
Roedtan	- 24, 62472	29.06759	975	Temperate interior
Sekgosese	- 23, 38483	30.17571	370	Hot interior
Xikundu	- 22, 8167	30, 8000	508	Hot interior

Xikundu falls at the latitude of 22.8167º, longitude 30.8000º with a minimum temperature of 21ºC and maximum of 38ºC, the place is composed more of small-scale farmers and they depend on the annual rainfall [55]. Considering all the stations, the highest altitude as illustrated on Table 3.1 is in Roedtan of about 975 m while the lowest altitude is of Mutale of about 329 m and the climatic conditions for these stations are classified as follows Ammondale and Roedtan are in the temperate interior while Mutale, Nwanedi, Sekgosese and Xikundu are in the hot interior; the temperature in those areas are always high compared to the ones in the temperate interior [56].

3.2 MODELS USED IN THIS SECTION

In the current study, a temperature-based model was used to estimate the global solar radiation in the Northern part of Limpopo province. This model as described in the last chapter was developed by Hargreaves and Samani in 1982 [57-58]. Currently, South Africa as a developing country cannot establish many meteorological weather stations to cover the whole area, especially in the remote rural areas. Thus the use of empirical relations comes in handy and gives advantages to solar energy technology developers around the country in those rural areas.

Hargreaves and Samani model use the observed temperature data and the empirical coefficients, K_r which depends on the regions (Coastal or Inland). The global solar radiation data (H) and temperature data were acquired from Agricultural Research Council (ARC) and South African Weather Services (SAWS). Six stations were selected with three years of data taken into consideration per station and the stations were classified according to their climatic conditions as illustrated in Table 1.

The major advantage of the Hargreaves and Samani model is that the value of K_r for a given area can be estimated. In the present investigation, the value of K_r was calculated for the six selected stations using the following equations [64],

$$K_r = 0.00185\,(T_{max} - T_{min})2 - 0.0433\,(T_{max} - T_{min}) + 0.04023, \quad (14)$$

where K_r is the empirical coefficients, T_{max} is the daily average maximum temperature and T_{min} is the daily average minimum temperature [66].

3.3 THE EXTRATERRESTRIAL SOLAR RADIATION (H_o)

The extraterrestrial solar radiation is the rate at which solar energy arrives on a horizontal surface at the top of the atmosphere [66]. It varies according to the latitude of the station, the distance of the Earth from the Sun, and the time of the year.

Therefore on any particular day, it varies from zero at sunrise to a maximum at noon and back to zero at sunset [59]. Solar radiation while passing through the Earth's atmosphere is subjected to the mechanisms of atmospheric absorption and scattering [60]. The daily extraterrestrial solar radiation on a horizontal surface, H_o, can be calculated as a function of the solar constant (I_{sc}), the latitude (ϕ) of the site of the area under study, the eccentricity correction factor of the Earth's orbit (E_o), the solar declination (δ) and the mean sunrise hour angle (ω_s) using Equation (1) [61, 62].

The values of extraterrestrial solar radiation (H_0) were computed for the different stations, understudy. The H_0 is an important parameter when estimating global solar radiation. H_0 on the horizontal surface was computed and the values were used to estimate the global solar radiation for the different stations. The H_0 depends on the declination angles and the latitude of the study area. On average the extraterrestrial irradiance is 1361 W/m^2. This value varies by ±3% as the Earth orbits the Sun. The Earth's closest approach to the Sun occurs around January 4th and it is furthest from the Sun around July 5th as reported by Wehrli in 1985. The extraterrestrial radiation can be computed as [62]:

$$H_0 = \frac{24}{\pi} I_{SC} E_0 \left(cos\delta * cos\emptyset * sin\omega_x + \frac{\pi W_x}{180} sin\emptyset * sin\omega_x \right) \quad (15)$$

where $E_0 = 1 + 0.033cos\frac{360n}{365}$ (16)

where I_{sc} is the solar constant defined as the amount of energy received at the top of the Earth's atmosphere measured at an average distance between the Earth and the Sun on a surface oriented perpendicular to the Sun. The generally accepted solar constant has been approximated as 1367 Wm^{-2} by the World Meteorological Organization (WMO), n = the day of the year, $1 \leq n \leq 365$, δ = solar declination angle, which can be expressed as follows [61,62]:

$$\delta = 23.45°sin\left[\frac{360}{365}(284+n)\right] \quad (17)$$

where, ϕ = latitude of the solar radiation station or site of study and ω_s= mean sunrise hour angle in degrees and is expressed as :

$$w_s = \arccos[-\tan(\phi)\cdot\tan(\delta)] \quad (18)$$

The sunset hour angle depends on the solar declination angle and latitude of the geographical study area and can be computed as

$$S_0 = \frac{2}{15}w_s \quad (19)$$

After the calculation of H_0, the temperature data for the three different years in each study area was used to estimate the global solar radiation (H). The K_r value used was obtained as suggested by Hargreaves and Samani [63]. To reach to a conclusion different statistical indicators were also calculated.

3.4 STATISTICAL ANALYSIS

In the current investigation three years' sample of measured global solar radiation data for each station were evaluated by comparing the data with the estimated data obtained using Hargreaves and Samani temperature based model. The validation of the model were achieve by using the following statistical tests: root mean square error (*RMSE*), mean bias error (*MBE*), mean percentage error (*MPE*) and Coefficient of determination (R^2) [64].

The root mean square error (RMSE) is defined as [65],

$$RMSE = \sqrt{\frac{\sum_{i=1}^{n}(H_{oi}-H_{Ei})}{n}}, \quad (20)$$

where H_{oi} and H_{Ei} are observed and estimated average values of global solar radiation for day *i* respectively and *n* is the total number observations [66].

The mean percentage error (MPE) is defined as [67],

$$MPE = \frac{1}{n}\left(\sum_{i=1}^{n}\frac{H_{oi}-H_{Ei}}{H_{oi}}\right)\times 100\%. \quad (21)$$

MPE test provides information on the short-term performance of the correlations by allowing a term-by-term comparison of the actual deviation between the calculated value and the measured value, the smaller the value, the better the model's performance [68].

However, the mean bias error (MBE) is defined as [69],

$$MBE = \sum_{i=1}^{n} \left(\frac{H_{oi} - H_{Ei}}{n} \right). \quad (22)$$

The *MBE* gives an idea of the divergence between the monthly average daily radiation values estimated by the model used and the measured values. A positive value shows overestimation and a negative value shows underestimation. Overestimation of an individual observation will cancel underestimation in a separate observation [70 - 71]. It gives the long term performance of the correlation by allowing a comparison of the actual deviation between calculated and measured values term by term.

The coefficient of determination, R^2, is used to analyze how differences in one variable can be explained by a difference in a second variable. The coefficient of determination is similar to the correlation coefficient, *R*. The correlation coefficient formula gives evidence of how strong linear relationship between two variables. R^2 is the square of the correlation coefficient (r), given by the equation (18) below [72],

$$R^2_{adjusted} = 1 - \frac{(1-r^2)(N-1)}{N-P-1} \ , \quad (23)$$

where *P* is the number of predictors and *N* is the total sample size. A simple MATLAB script was developed and used to compute the extraterrestrial solar radiation, which was used as an input together with the daily average minimum and maximum temperature data obtained for the different stations understudy to compute the global solar radiation. The interior value of K_r =1.6 was used. The different statistical measures were also evaluated to check the accuracy of the model in different climatic areas [73, 74].

In summary, in this chapter we were mainly focusing fully on the description of the study area based on the six station selected, the metereological data such as, minimum and maximum temperatures, the observation of the latitude, longitude and

altitude. Looked at the temperate interior and hot interior, applications of different models used to measure temperature and the confirmation of the suitability of the temperature based model, which was able to observe the temperatures between the lows and highs in those areas.

In the very same chapter it was also observed that the temperatures were low in Winter and high in Summer compared to other seasons. The use of different equations to arrive at the measured and observed temperatures and other metereological data including the determination of global solar radiation (H) and extraterrestrial solar radiation (H_0) using temperature based model were well monitored.

CHAPTER 4

In this chapter we will focus on the results and discussions, which will be based on the metereological data, temperature, extraterrestrial solar radiation (H_0), empirical constant (K_r), estimation of global solar radiation (H), the summary of the results and conclusion.

4. RESULTS AND DISCUSSIONS

The main purpose of the study was to test the applicability of the temperature-based model. The global solar radiation data for different stations were estimated and compared to the observed data. To arrive at a meaningful conclusions, the measured data and computed results where analysed using the following steps:

1. Analysis of the temperature data from the six selected stations and study area
2. Computing the K_r values from the different station
3. Computing the extraterrestial solar radiation for the study area
4. Computing the global solar radiation
5. Statistical analysis and comparison of the measured and computed values of global solar radiation

4.1 TEMPERATURE

Analysis of the maximum and minimum temperature for the six selected stations and its study areas are shown from tables 4.1 - 4.6 and it will be elaborated further below. Considering the station at Ammondale, its total bright sunshine hour in the year 2008, the minimum temperature was at 12,27 ^{0}C in Winter during the month of July and its maximum temperature in Summer of the month of March raised to 27,20 ^{0}C, hence in the year 2009 the temperatures dropped very much compared to the previous year (2008) because the minimum were reading 9,28 ^{0}C in Winter for the month of June which was the difference of 2,99 ^{0}C and its maximum wasn't that far different from the previous years as it was reading 27,73 ^{0}C and it is clearly that the temperatures has

changes less during this period in Summer. In 2010, the temperatures where very strange because the minimum increased to 11,82 ^{0}C in Winter for the month of July and the maximum to 28,55 ^{0}C in Summer for the month of January, which it was showing the causes of climate change impacting in South Africa, and has affected the intire ecosystem as patterned to the results in Table 4.1.

Table 4.2 for Mutale station shows the temperatures in year 2008 in Summer of the month of March were very high with the maximum of 29,20 ^{0}C and low in June during the Winter period with the minimum of 12,49 ^{0}C, again when looking at the year 2009, you will notice that there is a slide change in the minimum and the maximum temperatures they were both dropped compared to the year 2008, in June during Winter the minimum was reading 11,65 ^{0}C and the maximum in December during Summer was 29,02 ^{0}C there is always high temperature drop around June to August and high temperatures in December and January, therefore for the year 2010 in Winter during the month of July the temperatures were reaching 11,82 ^{0}C which was the lowest by then and 29,62 ^{0}C were the most highest, this area has the average values with similar trends during Summer.

The station in Nwanedi depicted in Table 4.3 shows that temperatures in the year 2008 in Autumn during the month of May were low at 14,04 ^{0}C and higher in Spring during the month of November at 29,10 ^{0}C, while in the year 2009, in Autumn of the month of May the minimum read 23,40 ^{0}C and during Summer of the month of February the maximum temperatures were reading 28,04 ^{0}C, therefore in 2010, the minimum temperatures were reading 11,82 ^{0}C in Winter during the month of July and the maximum temperatures at 28,55 ^{0}C in Summer of the month of January, this area has no trends in most of its seasonal values looking in all this years data from 2008 – 2010.

Table 4.4 which represents Roedtan station indicates that in Winter during the month of June the minimum temperatures were low at 16,42 ^{0}C and high in Summer during the month of December for the year 2008, in the year 2009 the minimum were the most lowest at 10,34 ^{0}C in Autumn for the month of March and high in Summer during the month of December at 31,09 ^{0}C, hence for the year 2010 the temperatures were reaching the lowest of 12,42 ^{0}C in Summer for the month of December and maximum of 33,17 ^{0}C in Spring during the month of September.

In Table 4.5, Sekgosese station reached the lowest temperature of 17,41 ^{0}C in Autumn for the month of April and the maximum of 29,31 ^{0}C in Spring for the month of November in the year 2008, in 2009 November the lowest was 10,34 ^{0}C in Spring and the maximum was 29,29 ^{0}C in Summer for the month of December and for year 2010, the lowest was at 12,42 ^{0}C in Summer for the month of December and highest 33,17 ^{0}C in January. Xikundu station in Table 4.6, depicted that the minimum temperature in Autumn for the month of March was 10,05 ^{0}C and the highest of 29,31 ^{0}C in Spring for the month of November in 2008, the similar trends shows again in the year 2009 during the Spring period of the month of September where it read 28,73 ^{0}C as the highest temperature and 10,34 ^{0}C as the lowest in Spring during the month of November. For the year 2010 during Autumn for the month of March it read 11,96 ^{0}C as the lowest and 31,17 ^{0}C as the maximum temperature during the month of September, we experiencing similar trends for both months of September and November for years 2008 to 2009.

The annual average temperature are shown on table 4.7. It is clear from the monthly average maximum and mimimum temperature that the highest values of temperature are in Summer and the lowest values are in Winter. Figures 4.1 and 4.2 illustrate the behaviour of the monthly minimum and maximum temperatures for the selected stations under study. The temperature start to increase from August to March and decrease from April to July each year. The high values of temperature are observed in December and January for most stations. The lowest values of the temperatures are observed in July, with the average annual temperatures ranging between 14 -18 ^{0}C. The graphs shows the intra-annual cycle in the temperature that is driven by radiation.

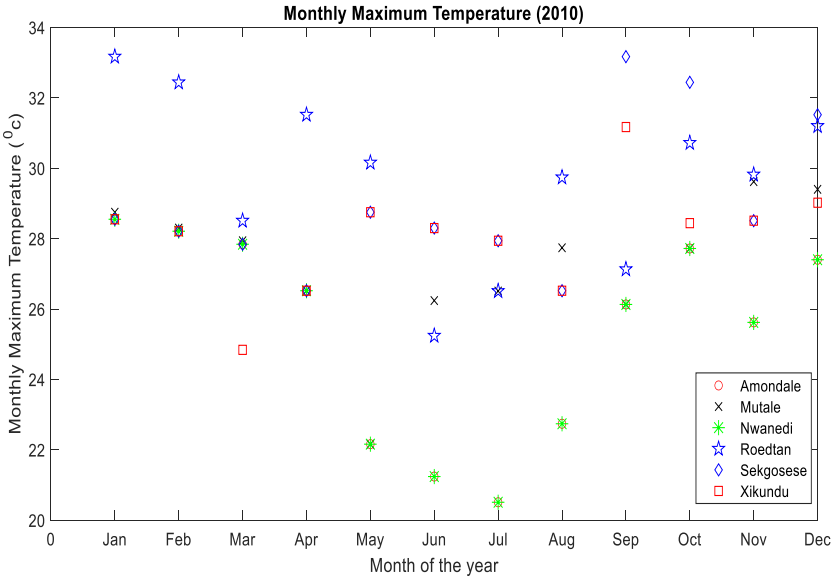

Figure 4.1. Average monthly minimum temperature for the stations under study for the year 2010

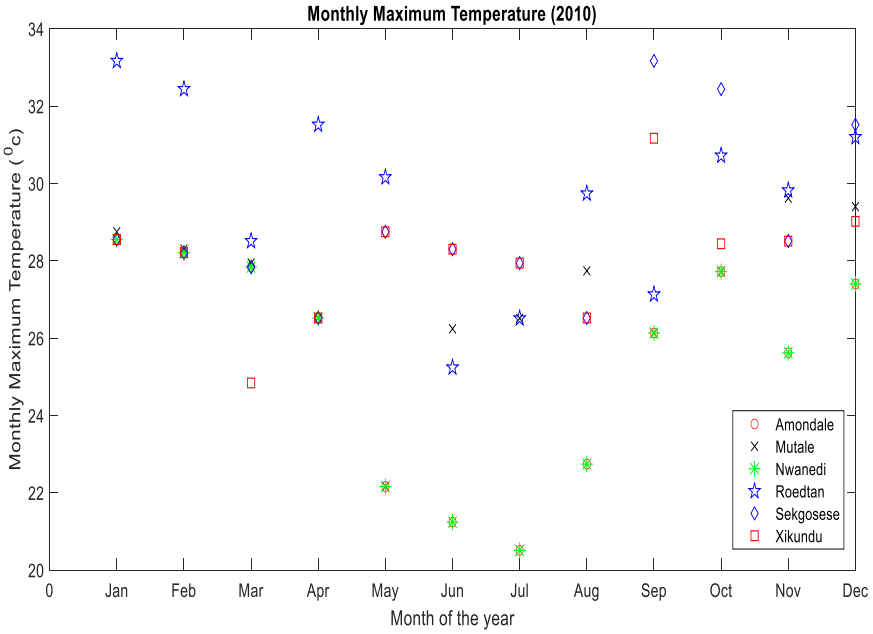

Figure 4.2. Average monthly maximum temperature for the stations under study for the year 2010

The maximum and minimum temperatures for each station are illustrated in Table 4.1 -4.6. It can be observed that the average temperature differs for each station, but some of these stations are not that far from each other, they mostly have similar trends, since they are within the same province. This is also in line with different climatic conditions. As mentioned above, the temperatures at all the stations vary seasonally as expected and illustrated in Figures 4.1 and 4.2 above. The lowest temperatures were obtained in Winter and maximum temperatures during Spring and Summer. For example, the maximum recorded temperature for Ammondale is about 28.55^{o}C and the minimum value is about 9.28^{o}C as shown in Table 4.1.

Table 4.1: Ammondale monthly average maximum and minimum temperature data for 2008 – 2010.

Year	2008		2009		2010	
Month	Maximum (°C)	Minimum (°C)	Maximum (°C)	Minimum (°C)	Maximum (°C)	Minimum (°C)
Jan	26.78	19.49	27.73	12.44	28.55	21.07
Feb	21.56	19.83	28.04	11.82	28.21	20.54
Mar	27.20	20.05	25.55	10.54	27.84	18.96
Apr	23.28	17.41	24.29	10.57	26.52	12.42
May	22.80	14.04	23.40	10.94	22.16	14.04
June	20.63	12.49	26.67	9.28	21.24	12.70
July	21.81	12.27	25.18	9.48	20.51	11.82
Aug	25.73	15.10	23.83	11.65	22.74	13.74
Sep	27.16	16.30	25.40	18.80	26.13	16.19
Oct	26.73	16.82	26.69	19.75	27.72	16.08
Nov	22.10	19.08	26.81	19.60	25.62	17.03
Dec	24.11	16.45	27.02	18.14	27.40	18.76

Table 4.2: Mutale monthly average maximum and minimum temperature data for 2008 – 2010.

Year	2008		2009		2010	
Month	Maximum (°C)	Minimum (°C)	Maximum (°C)	Minimum (°C)	Maximum (°C)	Minimum (°C)
Jan	27.78	18.42	27.73	13.44	28.75	17.07
Feb	23.66	19.73	28.04	15.82	28.30	21.54
Mar	29.20	21.85	25.55	16.54	27.94	18.90
Apr	28.28	17.41	24.29	18.57	26.52	17.42
May	27.80	18.04	26.40	19.94	22.16	17.04
June	25.63	12.49	26.67	17.28	26.24	13.70
July	26.81	13.27	26.18	16.48	26.51	11.82
Aug	26.73	15.10	27.83	11.65	27.74	13.74
Sep	29.16	16.30	27.40	18.80	26.13	16.19
Oct	26.73	16.82	28.69	19.75	27.72	16.08
Nov	28.10	19.08	29.81	15.60	29.62	17.33
Dec	28.11	17.45	29.02	19.14	29.40	18.11

The same goes for Mutale as illustrated in Table 4.2, the maximum temperature is about 29.62 °C and the minimum value is about 11.65 °C, while observing these two stations above there was a drastic drop during August in 2009 and 2010 almost all at 11 °C; similar trends were applicable for the month of May. During this period we normally expect lower actual sunshine hours than the other seasons. But the actual sunshine hours are rather more during the years under investigation in Winter and this may be attributed to limited absolute clear sky days for that particular year. In addition

to that, it is always preferable to calibrate the measuring instruments on regular basis to get a reliable set of data.

Unfortunately, the calibration records are not available for the area under study [48]. Similar trends of the temperature behaviour has been observed also at Nwanedi station. The station is situated in the Limpopo river basin and the Nwanedi river is surrounded by small scale farmers. The maximum and the minimum temperature values ranges between 9.28 ^{o}C in Winter for the month of June and 29.10^{o}C in Spring during the month of November as observed in Table 4.3 below. Similar trend of the change in the temperature was observed by Tshiala [77] and Mosase and Ahiablame [78]. The trends of the anualy temperature found in the Nwanedi statation coincide with the Mosase and Ahiablame studies [78].

Table 4.3: Nwanedi monthly average maximum and minimum temperature data for 2008 – 2010.

Year	2008		2009		2010	
Month	Max (°C)	Min (°C)	Max (°C)	Min (°C)	Max (°C)	Min (°C)
Jan	26.18	19.49	27.73	12.44	28.55	20.07
Feb	21.56	19.83	28.04	11.82	28.21	20.54
Mar	27.20	20.05	25.55	10.54	27.84	18.96
Apr	23.28	17.41	24.29	10.57	26.52	12.42
May	25.80	14.04	23.40	10.94	22.16	14.04
June	25.63	12.49	26.67	9.28	21.24	12.70
July	26.81	12.27	25.18	9.48	20.51	11.82
Aug	28.73	15.10	23.83	11.65	22.74	13.74
Sep	27.16	16.30	25.40	18.80	26.13	16.19
Oct	28.73	16.82	26.69	19.75	27.72	16.08
Nov	29.10	19.08	26.81	19.60	25.62	17.03
Dec	28.11	16.45	27.02	18.14	27.40	19.76

Table 4.4: Roedtan monthly average maximum and minimum temperature data for 2008 – 2010.

Year	2008		2009		2010	
Months	Maximum (°C)	Minimum (°C)	Maximum (°C)	Minimum (°C)	Maximum (°C)	Minimum (°C)
Jan	28.53	22.22	28.73	19.54	33.17	21.01
Feb	27.32	22.32	29.04	21.02	32.44	25.34
Mar	29.31	24.07	27.53	10.34	28.51	18.36
Apr	27.19	19.91	29.29	15.57	31.52	13.02
May	26.13	16.04	28.46	14.22	30.16	14.04
June	21.73	16.42	26.57	19.82	25.24	12.70
July	23.92	17.67	26.18	15.84	26.51	12.72
Aug	28.73	18.10	27.83	17.95	29.74	13.74
Sep	29.61	20.30	29.40	20.40	27.13	15.19
Oct	28.73	19.92	29.69	19.35	30.72	18.77
Nov	30.18	19.08	30.99	19.70	29.82	18.44
Dec	31.44	20.40	31.09	22.33	31.20	20.99

Table 4.5: Sekgosese monthly average maximum and minimum temperature data for 2008 – 2010.

Year	2008		2009		2010	
Month	Maximum (°C)	Minimum (°C)	Maximum (°C)	Minimum (°C)	Maximum (°C)	Minimum (°C)
Jan	26.78	19.49	27.73	12.44	28.55	21.07
Feb	21.56	19.83	28.04	11.82	28.21	20.54
Mar	27.20	20.05	25.55	10.54	27.84	18.96
Apr	23.28	17.41	24.29	10.57	26.52	12.42
May	27.78	18.42	27.73	13.44	28.75	17.07
June	23.66	19.73	28.04	15.82	28.30	21.54
July	26.20	21.85	25.55	16.54	27.94	18.90
Aug	28.28	17.41	24.29	18.57	26.52	17.42
Sep	28.53	22.22	28.73	19.54	33.17	21.01
Oct	27.32	22.32	29.04	21.02	32.44	25.34
Nov	29.31	24.07	27.53	10.34	28.51	18.36
Dec	27.19	19.91	29.29	15.57	31.52	13.02

Table 4.6: Xikundu monthly average maximum and minimum temperature data for 2008 – 2010.

Year	2008		2009		2010	
Month	Maximum (°C)	Minimum (°C)	Maximum (°C)	Minimum (°C)	Maximum (°C)	Minimum (°C)
Jan	25.68	19.49	27.73	12.44	28.55	21.07
Feb	26.56	19.83	28.04	11.82	28.21	20.54
Mar	25.20	10.05	25.55	11.00	24.84	11.96
Apr	24.19	17.41	24.29	10.57	26.52	12.42
May	26.77	18.42	27.73	13.44	28.75	17.07
June	23.09	19.73	28.04	15.82	28.30	21.54
July	27.20	21.85	25.55	16.54	27.94	18.90
Aug	28.28	17.44	24.39	19.27	26.52	17.42
Sep	27.59	22.22	28.73	19.54	31.17	21.01
Oct	27.92	22.32	29.04	21.02	28.44	25.34
Nov	28.91	24.07	27.53	10.34	28.51	18.36
Dec	26.98	20.91	28.24	19.57	29.02	23.02

Tables 4.1 – 4.6 show similar trends of the seasonal variation of the temperature with the minimun temperatures obtained in Winter and the maximun temperatures obtained in Summer. In Roedtan the minimum temperatures range between 10.34°C – 19.70°C during winter and sommer seasons. Sometimes the minimum temperature value is recorded to a lower value due to other factors affaecting the temperature like rain, wind,cloud cover, etc. The Roedtan average monthly temperatures are tableted in Table 4.4. Temperatures in Sekgosese range between 10.54 °C – 31.52°C for the

three years as shown in Table 4.5 and Xikundu is between 10.05^{o}C – 29.31^{o}C as shown in Table 4.6. From all the stations understudy we can observe that there are factor affecting the temperature due to the area where the station is situated and the landscape. Some of the stations are situated in the mountaneous region and some are closer to the rivers.

Table 4.7: Average yearly maximum and minimum temperature data for 2008-2010.

Year	2008		2009		2010	
Station	Max (^{o}C)	Min (^{o}C)	Max (^{o}C)	Min (^{o}C)	Max (^{o}C)	Min(^{o}C)
Ammondale	24.16	16.62	25.89	13.58	25.39	16.12
Mutale	27.49	17.16	27.30	16.92	27.25	16.58
Nwanedi	26.57	16.61	25.88	13.58	25.39	16.11
Roedtan	27.74	20.54	28.73	18.17	29.64	17.03
Sekgosese	26.43	20.23	27.15	14.68	29.02	18.80
Xikundu	26.05	16.36	25.48	13.85	25.19	17.71

Table 4.7 shows how the yearly average minimum and maximum temperatures for 2008 - 2010 vary in different regions, due to different landscapes. Ammondale, Nwanedi, and Xikundu station had a temperature that ranges between 13.58^{o}C to 26.57^{o}C, the results are in agreement particularly when observing the stations locations. While Roedtan and Sekgosese read between 14.68^{o}C to 29.64^{o}C, these two are far apart from the other stations mentioned above, and Mutale is unique from almost all the stations since it is situated in the far North of the Limpopo province with the range from 16.58 ^{o}C to 27.49^{o}C.

4.2 EXTRATERRESTRIAL SOLAR RADIATION

As illustrated under methodology one of the important input needed to compute the global solar radiation (H) is the extraterrestrial solar radiation (H_0) data which can be computed using equation (1). The extraterrestrial solar radiation on a horizontal

surface H_0 is considered as a function of only latitude, φ. As solar radiation passes through the Earth's atmosphere, it is further modified by the processes of scattering and absorption due to the presence of cloud and atmospheric particles. Consequently the daily global solar irradiation flux incident on a horizontal surface is very much location specific and less than the extraterrestrial irradiation. The mean daily extraterrestrial solar irradiation on the horizontal surface, H_0 in MJm^{-2} day^{-1} integrated over the period of sunrise to sunset per station under study is computed for each day of the year. The computed values of H_0 for the six stations under study and for the year 2008 – 2010 are tablated from Tables 4.8 – 4.9 and represented by Figures 4.3 – 4.8 and are well explained.

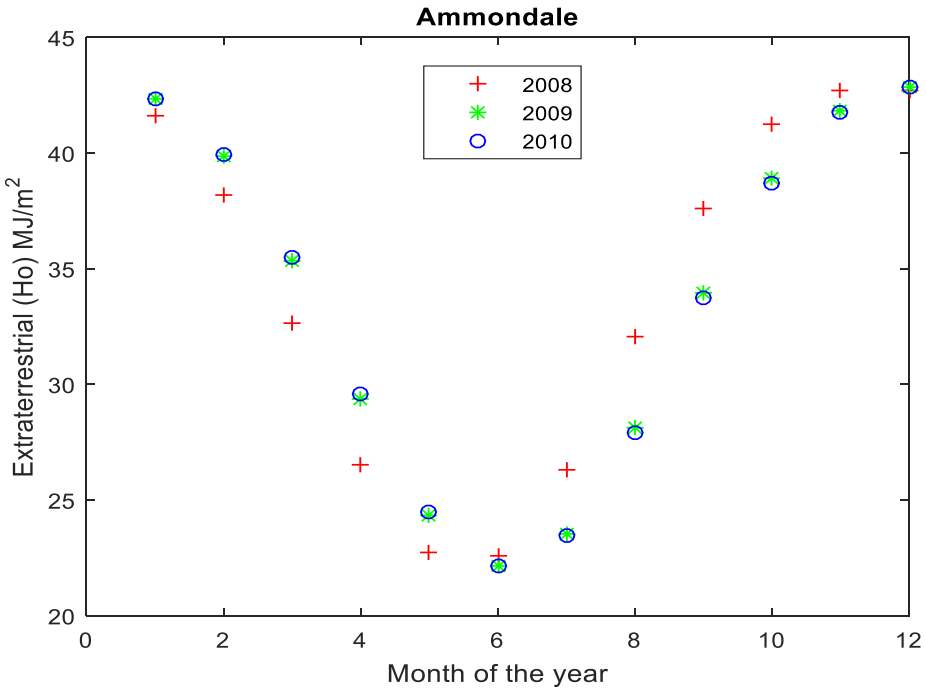

Figure 4.3: Computed monthly average extraterrestrial solar radiation for the year 2008 – 2010 for Ammondale station.

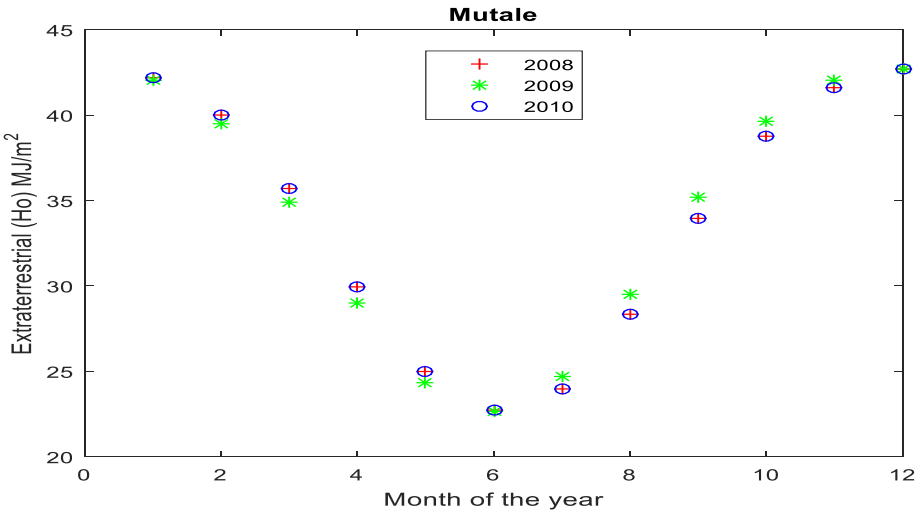

Figure 4.4: Computed monthly average extraterrestrial solar radiation of Mutale station for the year 2008 – 2010.

Table 4.8: Computed monthly average extraterrestrial solar radiation of Ammondale for the year 2008 – 2010.

Year	2008	2009	2010
Month	H_0 (MJ/m^2)	H_0 (MJ/m^2)	H_0 (MJ/m^2)
Jan	41.61	42.31	42.34
Feb	38.15	39.86	39.96
Mar	32.61	35.31	35.47
Apr	26.54	29.37	29.56
May	22.71	24.35	24.49
June	22.62	22.14	22.16
July	26.28	23.57	23.44
Aug	32.09	28.13	27.88
Sep	37.63	33.97	33.71
Oct	41.22	38.89	38.69
Nov	42.72	41.84	41.75
Dec	42.74	42.88	42.87

Table 4.9: Computed monthly average extraterrestrial solar radiation for Mutale station for the year 2008 – 2010.

Year	2008	2009	2010
Month	H_0 (MJ/m^2)	H_0 (MJ/m^2)	H_0 (MJ/m^2)
Jan	42.21	42.04	42.21
Feb	39.98	39.51	39.98
Mar	35.69	34.89	35.69
Apr	29.96	29.03	29.96
May	25.00	24.34	25.00
June	22.70	22.67	22.70
July	23.96	24.67	23.96
Aug	28.32	29.53	28.32
Sep	33.98	35.22	33.98
Oct	38.76	39.63	38.76
Nov	41.64	42.04	41.64
Dec	42.68	42.71	42.68

The extraterrestrial global solar radiation changed regularly with season for all selected stations as illustrate in Tables 4.8 - 4.14 for all the year under study (2008-2010). Ammondale station received the minimum of 22.62 MJ/m^2, 22.14 MJ/m^2 and 22.16 MJ/m^2 which were the lowest values found in the month of June in winter from 2008 – 2010 respectively and with the highest values of 42.74 MJ/m^2, 42.88 MJ/m^2 and 42.87 MJ/m^2 during the month of December and January as shown in Table 4.8 and graphically presented in Figure 4.3. Mutale station received the high H_0 during Summer time, but lower value compared to Ammondale during November, December and January. It also received the lowest recorded values Autumn and Winter during May, June and July. The lowest values obtained were about 22.70 MJ/m^2 22.67 MJ/m^2 and 22.70 MJ/m^2 and the highest value 42.68 MJ/m^2 , 42.71 MJ/m^2 and 42.68 MJ/m^2

respectively as illustrated in Table 4.9 and Figure 4.4. The values obtained for Ammondale and Mutale are almost the similar particularly the ones around the months of June and December for the year 2008 – 2010 since they are experiencing similar rainfall.

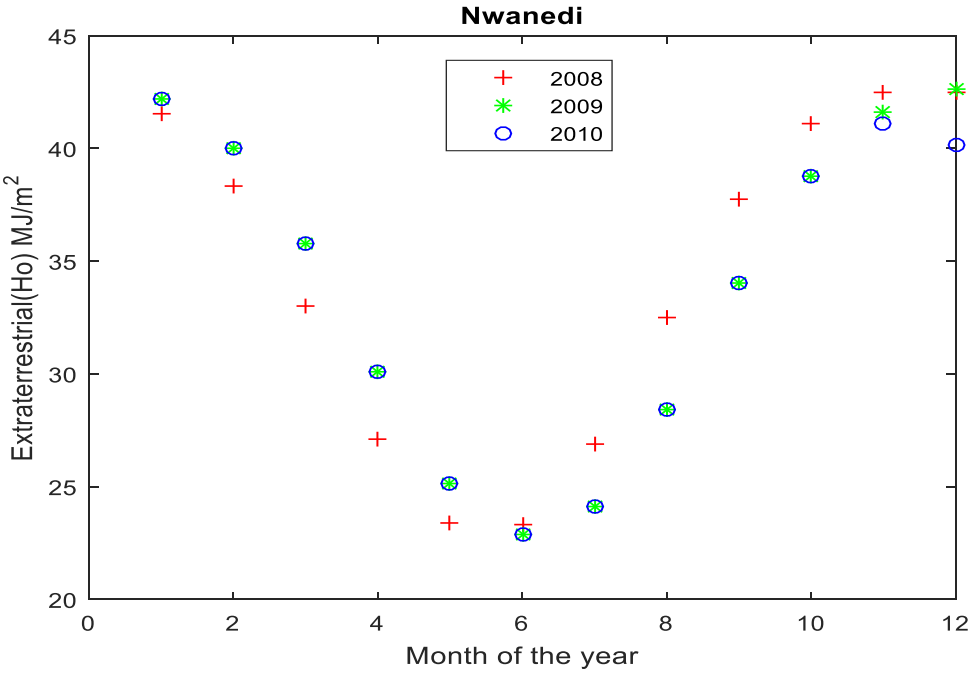

Figure 4.5: Computed monthly average extraterrestrial solar radiation of Nwanedi station for the year 2008 – 2010.

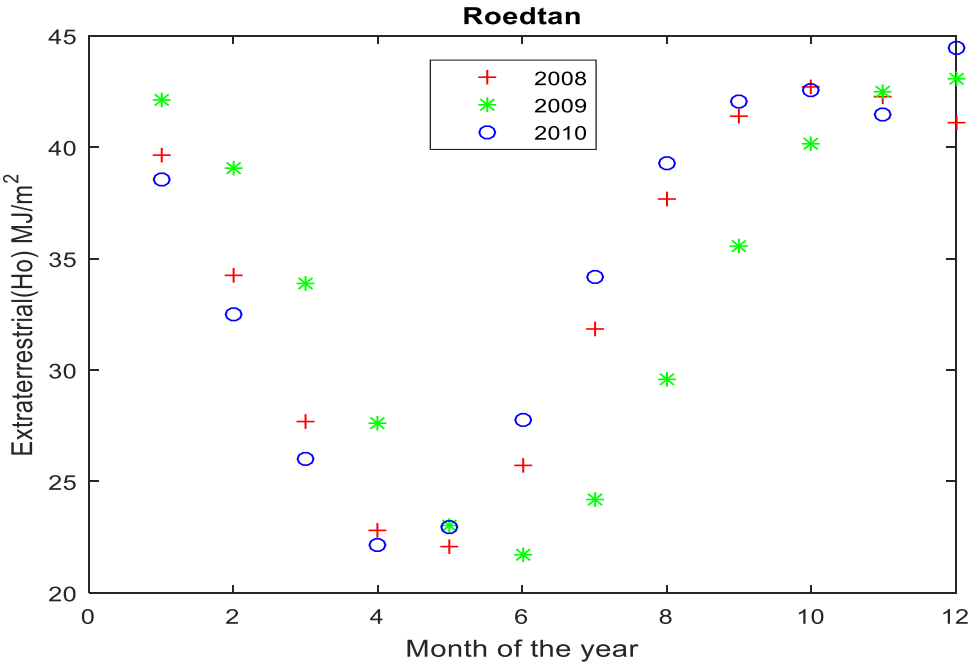

Figure 4.6: Computed monthly average extraterrestrial solar radiation of Roedtan for the year 2008 – 2010.

Table 4.10: Computed monthly average extraterrestrial solar radiation of Nwanedi station for the year 2008 – 2010.

Year	2008	2009	2010
Month	H_0 (MJ/m^2)	H_0 (MJ/m^2)	H_0 (MJ/m^2)
Jan	41.51	42.17	42.17
Feb	38.31	39.98	39.98
Mar	33.03	35.76	35.76
Apr	27.14	30.08	30.08
May	23.40	25.14	25.14
June	23.31	22.85	22.85
July	26.87	24.10	24.10
Aug	32.49	28.44	28.44
Sep	37.76	34.05	34.05
Oct	41.10	38.78	38.78
Nov	42.48	41.61	41.12
Dec	42.52	42.63	40.12

Nwanedi station received minimum values ranging from 22.85 MJ/m^2 to 26.87 MJ/m^2 between the months of May, June and July and maximum values between the months of October, November, December and January from 38.78 MJ/m^2 to 42.63 MJ/m^2 in the year 2008-2010 as shown in Table 4.10, as illustrated in figure 4.5. The Roedtan values of H_0 reached the highest of 44.47 MJ/m^2 during the month of December 2010 and 43.05 MJ/m^2 during the month of December 2009 and the recorded lowest values were 22.11 MJ/m^2 in Autumn during the month of May of the year 2008 as in Table 4.11. Similar trends were happening during the year 2009 and 2010 in the month of February where it has recorded 39.78 MJ/m^2 and 39.96 MJ/m^2 as shown in Table 4.11 and graphically represented in Figure 4.6. It is normally windy during the month of August; therefore, the wind might have contributed to this deviation whereby the

readings were very low. It can be observed that the global solar radiation predicted using temperature-based models gave a good relationship.

Table 4.11: Computed monthly average extraterrestrial solar radiation of Roedtan for the year 2008 – 2010.

Year	2008	2009	2010
Month	H_0 (MJ/m^2)	H_0 (MJ/m^2)	H_0 (MJ/m^2)
Jan	39.66	42.12	38.58
Feb	34.23	39.06	32.53
Mar	27.66	33.85	26.03
Apr	22.79	27.62	22.17
May	22.11	22.99	22.97
June	25.69	21.69	27.76
July	31.82	24.22	34.16
Aug	37.65	29.57	39.31
Sep	41.36	35.58	42.07
Oct	42.74	40.12	42.54
Nov	42.24	42.52	41.47
Dec	41.10	43.05	44.47

Table 4.12: Computed monthly average extraterrestrial solar radiation of Sekgosese station for year 2008 – 2010.

Year	2008	2009	2010
Month	H_0 (MJ/m^2)	H_0 (MJ/m^2)	H_0 (MJ/m^2)
Jan	39.00	42.23	42.30
Feb	33.39	39.78	39.96
Mar	27.03	35.23	35.55
Apr	22.97	29.32	29.70
May	23.36	24.39	24.67
June	27.75	22.32	22.35
July	33.89	23.89	23.62
Aug	38.95	28.52	28.03
Sep	41.74	34.32	33.80
Oct	42.43	39.09	38.72
Nov	41.62	41.89	41.71
Dec	42.46	42.83	42.81

There were a similar trend observed for the highest values obtained during the month of November 2008 – 2010 ranging from 41.62 MJ/m^2 to 41.89 MJ/m^2 and same goes to December 2008- 2010, the values were reading 42.46 MJ/m^2 to 42.81 MJ/m^2 with the lowest of 22.32 MJ/m^2 for Sekgosese as in Table 4.12, well shown in Figure 4.7. The highest value of extraterrestrial solar radiation was 42.70 MJ/m^2 during the period of December of the year 2008 and 22.67 MJ/m^2 for Xikundu stations respectively as demonstrated in Figure 4.8 and Table 4.13. It is evident from the tables that the computed values of H_0 at each given stations are very close to each other. Even when we still observe variations in the monthly average extraterrestrial solar radiation, but the obtained values from each stations show that, there is a slight difference in the factor affecting H_0 values [48]. All the stations H_0 depend on the seasons, which shows

the similar trends obtained when working with the maximum and minimum temperatures for all the stations.

Table 4.13: Computed monthly average extraterrestrial solar radiation of Xikundu for the year 2008 – 2010.

Year	2008	2009	2010
Month	H_0 (MJ/m^2)	H_0 (MJ/m^2)	H_0 (MJ/m^2)
Jan	42.22	40.08	42.15
Feb	39.97	35.32	39.80
Mar	35.68	29.12	35.37
Apr	29.94	24.10	29.57
May	24.97	22.91	24.70
June	22.67	25.90	22.64
July	23.93	31.55	24.19
Aug	28.29	37.16	28.77
Sep	33.96	40.83	34.47
Oct	38.76	42.37	39.12
Nov	41.65	42.20	41.82
Dec	42.70	42.12	42.71

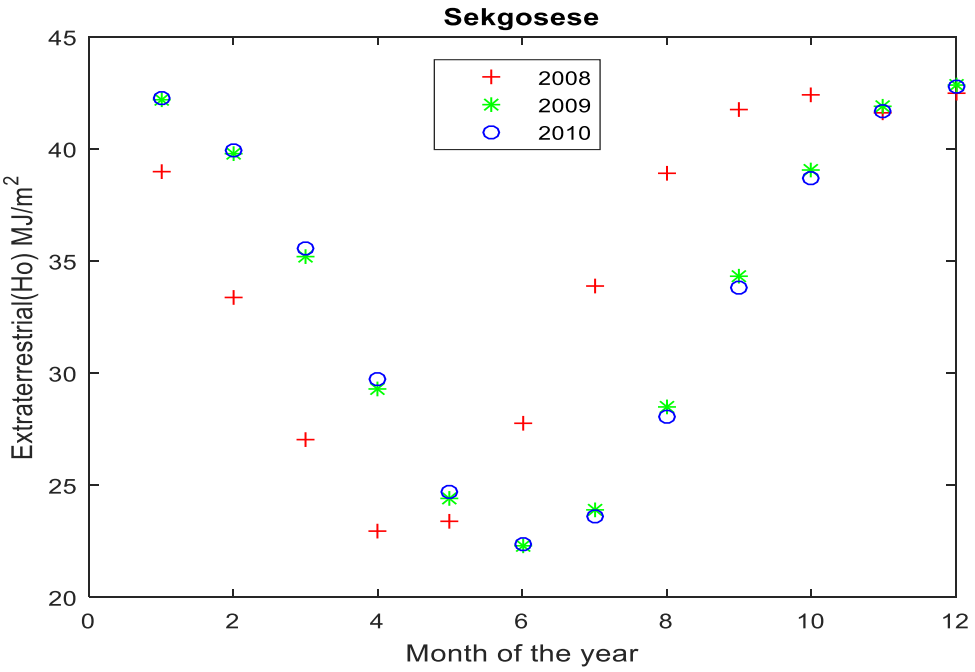

Figure 4.7: Computed monthly average extraterrestrial solar radiation of Sekgosese station for the year 2008 – 2010.

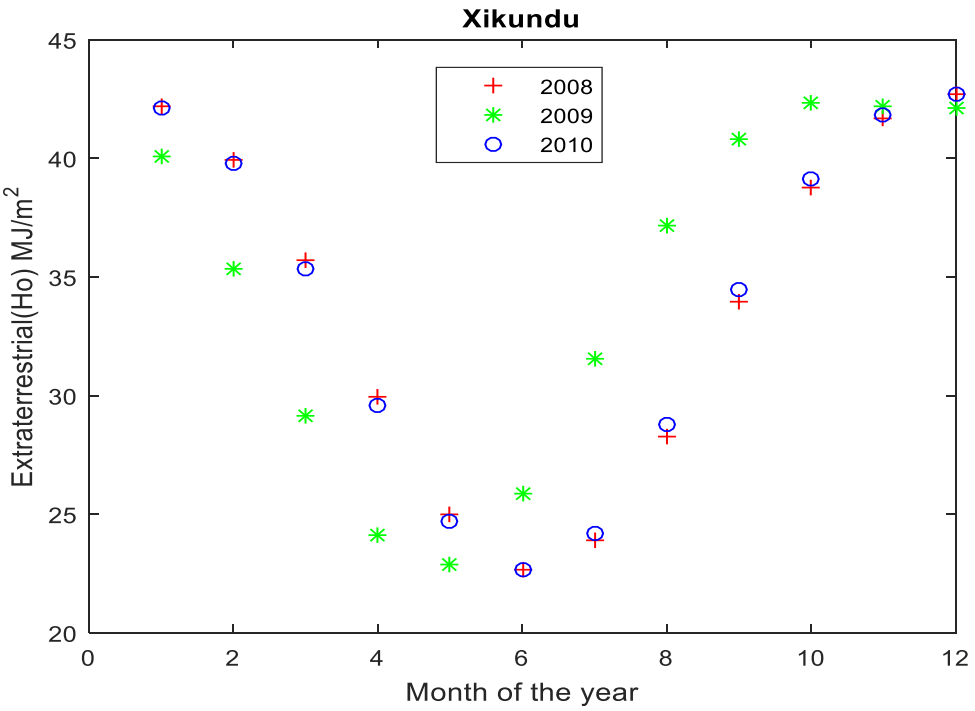

Figure 4.8: Computed monthly average extraterrestrial solar radiation of Xikundu for the year 2008 – 2010.

The other factors involved in the computing of the H_0 is the solar declination and the sunshine hours angle. During Winter season we normally expect lower actual sunshine hours than the other seasons. Sometimes, the actual sunshine hours are rather more during a particular year compare to the Winter of another year and sometimes some of the years has limited absolute clear sky days [48]. Table 4.14, shows the yearly average values for H_0 in different stations from the year 2008 – 2010. If can be observed that the values are amost similar for all stations.

Table 4.14: Yearly average values for H_0 (MJ/m^2)for different stations.

Station	2008	2009	2010
Ammondale	33.91	33.56	33.53
Mutale	33.74	33.87	33.74
Nwanedi	34.16	33.78	33.57
Roedtan	34.09	33.53	34.51
Sekgosese	34.56	33.65	33.67
Xikundu	33.73	34.48	33.78

4.3 EMPIRICAL CONSTANT (K_r)

The equestion developed by Samani to provide a modification of the empirical coefficient was used in this study to compute the empirical coefficient at each station. The relation suggests that K_r is a function of the daily temperature range. The modification of the equation is based on the fact that it will minimize the error associated with estimation of the solar radiation. The minimum and maximun temperature values reported in Tables 4.1 – 4.6 were used. The values obtained for K_r are given in Table 4.15. It can be observed for each station under study that the value of K_r is in good agreement with the value reported by Hargreaves and Samani [6]. From the table, it can be deduced that the temperature data obtained from the different stations can be used to estimate the value of K_r for the inland region.The yearly average values of K_r obtained for each station are similar to the values suggested for the inland regions, and thus the Samani temperature dependent equation can be used to estimate the value of K_r in the Northern region of Limpopo province. It can be observed from the table that during some of the months the calculated value of K_r are slightly different from the average values, the difference may

be encountered because of the change in temperature and other parameters like the cloud cover, humidity, rain fall, etc., on some of the days during the months.

Table 4.15: Calculated monthly K_r stations understudy (2010).

Month	Ammondale	Mutale	Nwanedi	Roedtan	Sekgosese	Xikundu
Jan	0.16	0.16	0.15	0.15	0.15	0.15
Feb	0.15	0.15	0.15	0.15	0.15	0.16
Mar	0.16	0.16	0.15	0.16	0.15	0.16
Apr	0.16	0.16	0.16	0.16	0.16	0.16
May	0.15	0.16	0.16	0.16	0.16	0.16
Jun	0.15	0.16	0.15	0.16	0.15	0.15
Jul	0.16	0.16	0.16	0.16	0.16	0.16
Aug	0.15	0.16	0.15	0.15	0.15	0.15
Sep	0.16	0.16	0.16	0.15	0.15	0.16
Oct	0.16	0.16	0.16	0.16	0.15	0.16
Nov	0.16	0.15	0.15	0.16	0.16	0.16
Dec	0.15	0.16	0.16	0.16	0.15	0.16
Average	0.16	0.16	0.16	0.16	0.16	0.16

4.4 ESTIMATION OF GLOBAL SOLAR RADIATION (H)

The main aim of the study was to estimate the global solar radiation (H) using the temperature measured data. Hence from the analysis of the temperature data, it was found that the temperature changes based on the change in the seasons of the year. The higher temperature are obtained in Summer and lower temperature in Winter. The performance of the Hargreaves and Samani temperature based model for the stations under study were tested using the 2008 - 2010 temperature data. The results are reported using the tables and are graphically represented, where the average daily

observed and the estimated global solar radiation were compared. The graphical representations of the comparison of the average daily measured and estimated global solar radiation are shown in the figures below and the values are demonstrated in the tables below.

Table 4.16: Ammondale monthly average global solar radiation measured and estimated for 2008 – 2010.

Year	2008		2009		2010	
Month	Measured (MJ/m^2)	Estimated (MJ/m^2)	Measured (MJ/m^2)	Estimated (MJ/m^2)	Measured (MJ/m^2)	Estimated (MJ/m^2)
Jan	16.48	19.49	17.73	12.44	18.55	21.07
Feb	21.06	24.83	18.04	11.82	18.21	20.54
Mar	17.40	20.05	15.55	10.54	16.84	18.96
Apr	16.28	17.41	14.29	10.57	11.52	12.42
May	12.80	14.04	13.40	10.94	12.16	14.04
June	11.63	12.49	11.67	9.28	11.24	12.70
July	11.51	12.27	11.18	9.48	10.51	11.82
Aug	14.73	15.00	13.83	11.65	12.74	13.74
Sep	16.16	16.30	15.40	18.80	16.13	16.19
Oct	16.73	16.82	16.69	19.75	17.72	16.08
Nov	16.10	13.08	16.81	19.60	15.62	17.03
Dec	18.11	24.45	20.02	24.14	17.40	18.76

Table 4.16 Shows the measured and estimated global solar radiation for Ammondale stations. It can be observed that there is a good agreement between the measured and estimated global solar radiation values for each year. The maximum values are obtained in Summer and the minimum values are obtained in Winter, they range from 9.28 MJ/m^2 to 24.83 MJ/m^2 between the years 2008 – 2010. The comparison of the

measured and the estimated global was also depicted graphically, i.e. Figures 4.9 - 4.11 show the comparisons between the calculated global solar radiation from temperature data and the measured global solar radiation for Ammondale station, it is clear from the figures that there is a good agreement between the calculated and measured global solar radiation.

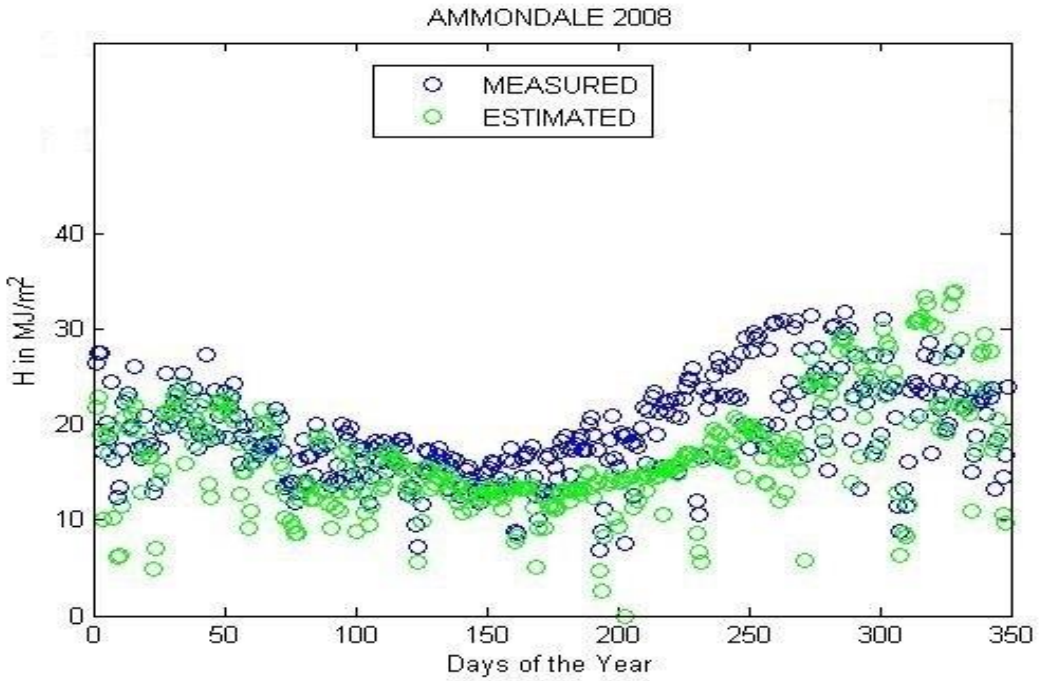

Figure 4.9: Comparisons between the estimated and the measured global solar radiation for Ammondale station (2008).

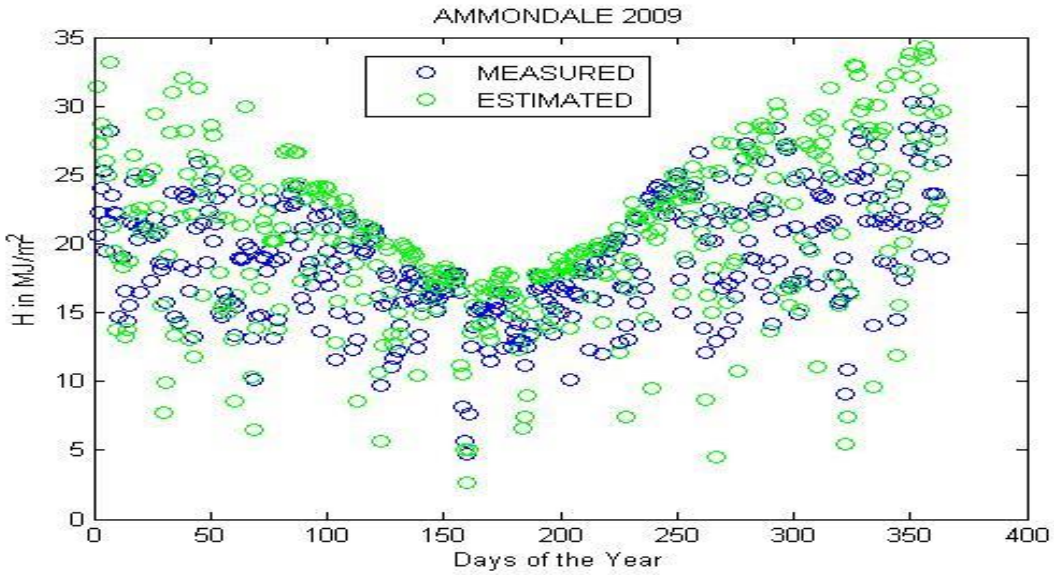

Figure 4.10: Comparisons between the estimated and the measured global solar radiation for Ammondale station (2009).

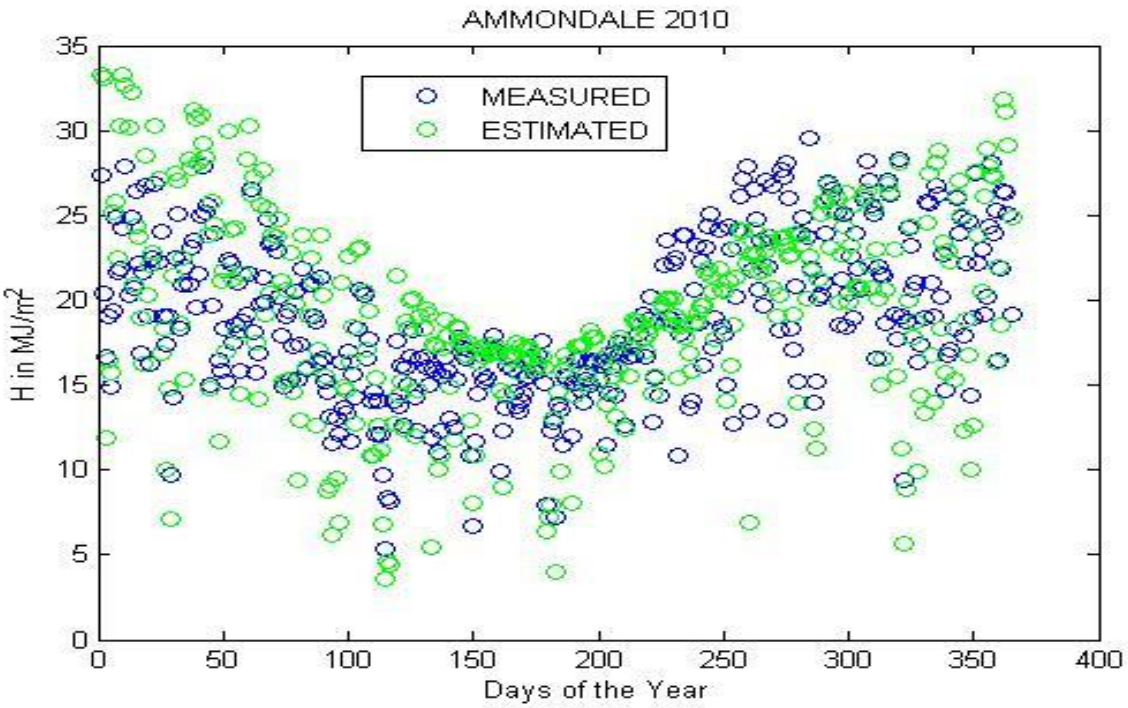

Figure 4.11: Comparisons between the estimated data and the measured global solar radiation for Ammondale station (2010).

Table 4.17: Average values for statistical tests.

Year	Station	RMSE	MBE	MPE	R^2
2008	Ammondale	0,0144	0,0072	0,7152	0,9103
2009	Ammondale	0,0105	-0,0044	-0,4365	0,9652
2010	Ammondale	0,0193	-9,2719e-004	0,8629	0,9627

The yearly trends of the global solar radiation is similar to the trends obtained for the yearly maximum and minimum temperatures. The statistical comparison between the measured and estimated global solar radiation was performed as shown in Table 4.17. The table represents the Mean Percentage Error (*MPE*), Mean biased Error (*MBE*) and Root Mean Square Error (*RMSE*) values, Th value of the RMSE is about 0.0105 for 2009 and the obtained MBE and MPE values are -0.0044 and -0.4365 respectively. The R^2 value is 0.9103 which is approximately equal to 1 as expected for all the years. Hence for the year 2008 – 2010 the value ranges from 0.0144 to 0.0193 for RMSE, 0.0044 to -9.2719e-004 for MBE, 0.4365 to 0.8629 for MPE and R^2 being 0.9103 to

0.9652. The trend of the small values of the MBE, MPE and RMSE illustrate a good agreement of the measured and estimated global solar radiation. As the coefficients of determination and correlation coefficients R^2 is close to 1, the results emphesise that indeed there is a good agreement between the measured and estimated global solar radiation data. Similar trends of the behaviour of the global solar radiation has been observed in Mutale stations. From Table 4.18, it can be seen that there is a good coalition between the measured and estimated global solar radiation values for each year understudy. The maximum values are obtained in Summer and the minimum values are obtained in Winter, they range from 9.51 MJ/m^2 to 25.40 MJ/m^2 between the years 2008 – 2010.

Table 4.18: Mutale monthly average global solar radiation for measured and estimated data from 2008 – 2010.

Year	2008		2009		2010	
Month	Measured (MJ/m^2)	Estimated (MJ/m^2)	Measured (MJ/m^2)	Estimated (MJ/m^2)	Measured (MJ/m^2)	Estimated (MJ/m^2)
Jan	18.53	22.22	18.73	19.54	22.17	21.01
Feb	24.32	22.32	19.04	21.02	22.44	25.34
Mar	19.31	24.07	12.53	10.34	19.51	18.36
Apr	17.19	19.91	19.29	15.57	12.52	13.02
May	16.13	26.04	15.46	14.22	15.16	14.04
June	10.73	16.42	18.57	19.82	15.24	12.70
July	13.92	17.67	13.18	11.84	9.51	12.72
Aug	23.73	18.10	16.83	17.15	12.74	13.74
Sep	14.61	20.30	21.40	20.80	23.13	15.19
Oct	18.73	19.92	19.69	19.05	20.72	18.77
Nov	16.18	19.08	20.99	19.70	22.32	18.44
Dec	20.44	25.40	25.09	24.33	25.20	22.99

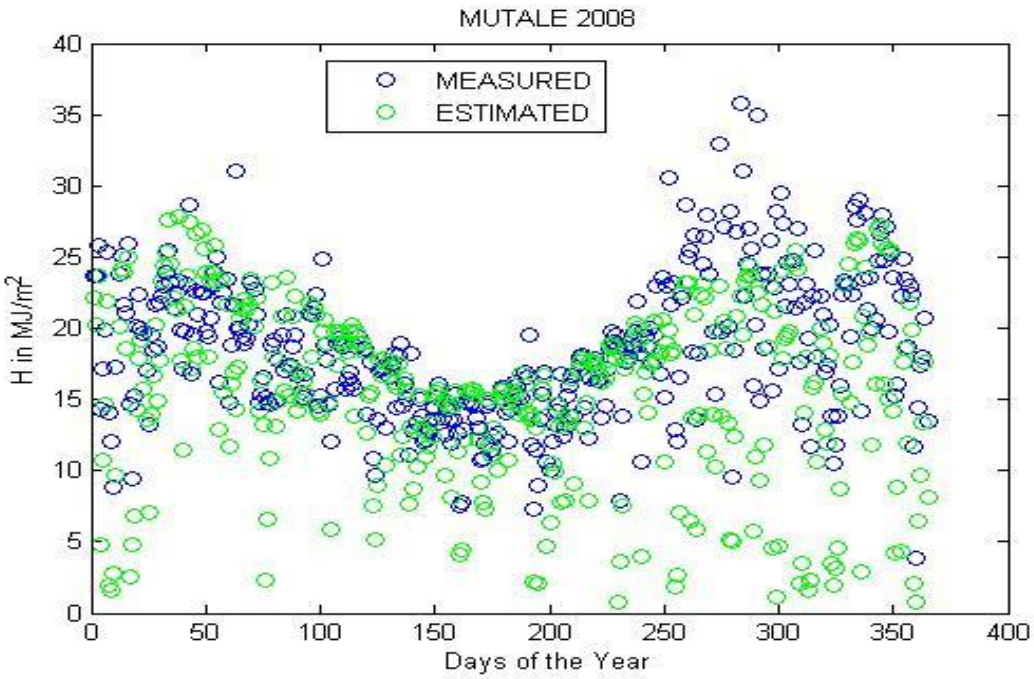

Figure 4.12: Comparisons between the estimated and the measured global solar radiation for Mutale station (2008).

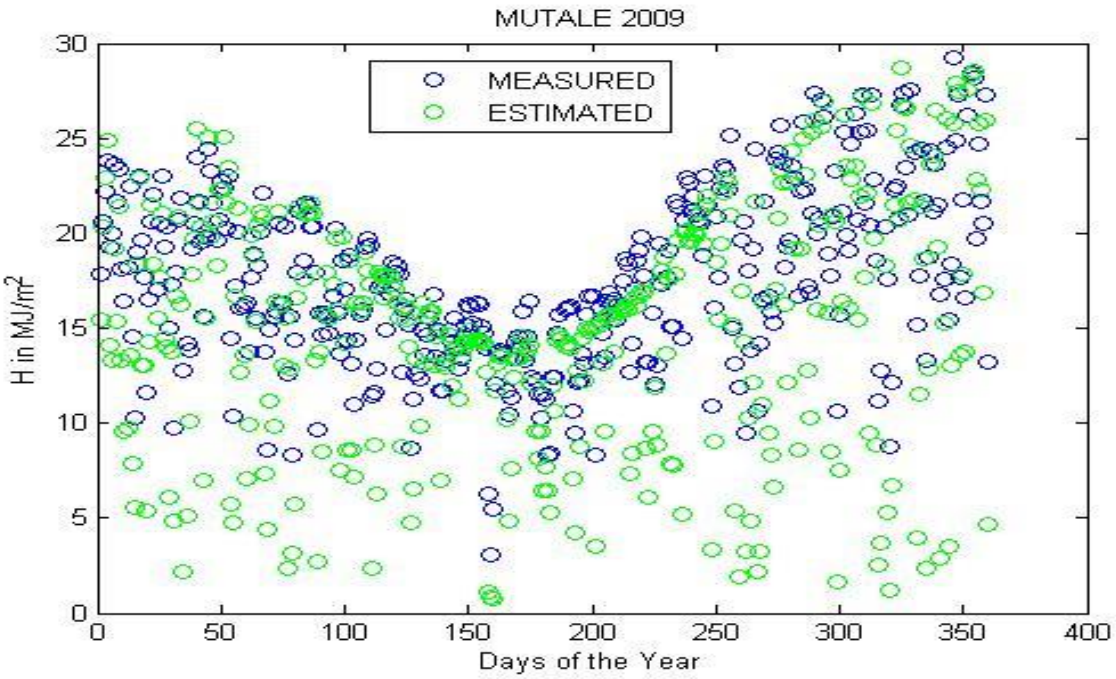

Figure 4.13: Comparisons between the estimated and the measured global solar radiation for Mutale station (2009).

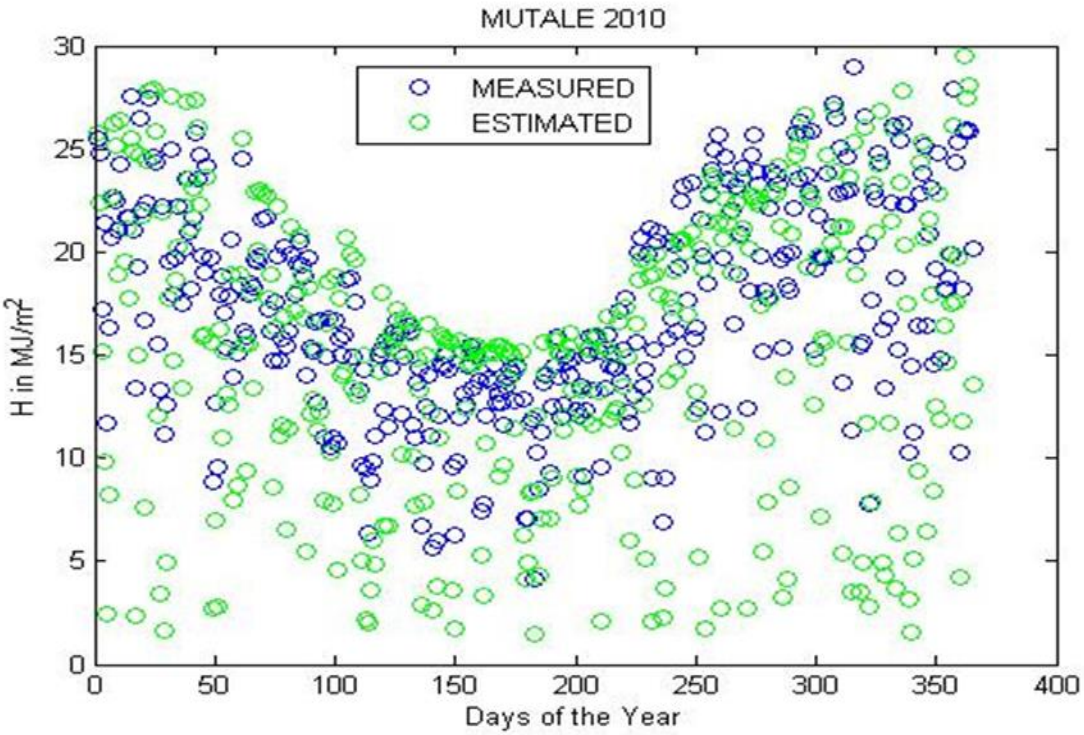

Figure 4.14: Comparisons between the estimated and the measured global solar radiation for Mutale station (2010).

Table 4.19: Average values for statistical tests.

Year	Station	RMSE	MBE	MPE	R^2
2008	Mutale	0,0146	0,0080	0,7967	0,8824
2009	Mutale	0,0115	0,0071	0,7124	0,9708
2010	Mutale	0,0115	0,0058	0,5818	0,9225

Figures 4.12 – 4.13 represents the comparisons between the estimated and measured gloal solar radiation for Mutale station. The yearly trends of global solar radiation is the same compared to Ammondale station. Table 4.19 represents the *MPE*, *MBE* and *RMSE* values. As observed from the table, for the year 2008, the values for the statistical comparison are obtained as RMSE = 0, 0146, MBE = 0, 0080, MPE = 0,7967 and R^2 = 0, 8824. For the year 2008 – 2010 the value ranges from RMSE= 0, 0115 to 0, 0146, MBE= 0, 0058 to 0, 0080, MPE= 0, 5818 to 0, 7967 and R^2 = 0, 8824 to 0, 9708.

Table 4.20: Nwanedi monthly average global solar radiation for measured and estimated data from 2008 – 2010.

Year	2008		2009		2010	
Months	Measured (MJ/m^2)	Estimated (MJ/m^2)	Measured (MJ/m^2)	Estimated (MJ/m^2)	Measured (MJ/m^2)	Estimated (MJ/m^2)
Jan	17.75	25.71	19.23	17.44	19.95	25.00
Feb	22.15	26.87	19.04	18.82	18.21	20.54
Mar	18.85	25.09	25.58	10.54	16.84	19.76
Apr	18.89	21.71	24.29	20.57	18.52	15.49
May	12.80	14.04	27.40	22.94	17.16	16.04
June	17.63	12.49	21.47	19.28	11.24	18.70
July	15.78	12.87	21.18	19.48	10.51	14.82
Aug	18.73	15.80	13.83	18.65	16.74	13.94
Sep	17.18	18.30	16.49	19.80	16.93	14.59
Oct	19.93	16.82	23.69	19.99	14.72	18.18
Nov	25.10	26.08	28.81	22.60	20.08	18.77
Dec	18.34	16.98	24.57	23.78	19.82	19.88

Table 4.20 shows the average monthly estimated and measured values for Nwanedi station, it can be observed that there is a good consensus between the measured and estimated global solar radiation values for each year. The maximum values of the global solar radiation are obtained in Summer and the minimum values are obtained in Winter respectively as found in the other stations, they range from minimum value of 10.51 MJ/m^2 to a mximum value of 28.81 MJ/m^2 between the year 2008 – 2010. Figures 4.15 – 4.17 shows the scatter plots of the estimated and measured daily average global solar radiation for each year. The figures illustrate that there is a good treaty between the estimated and measured global solar radiation.

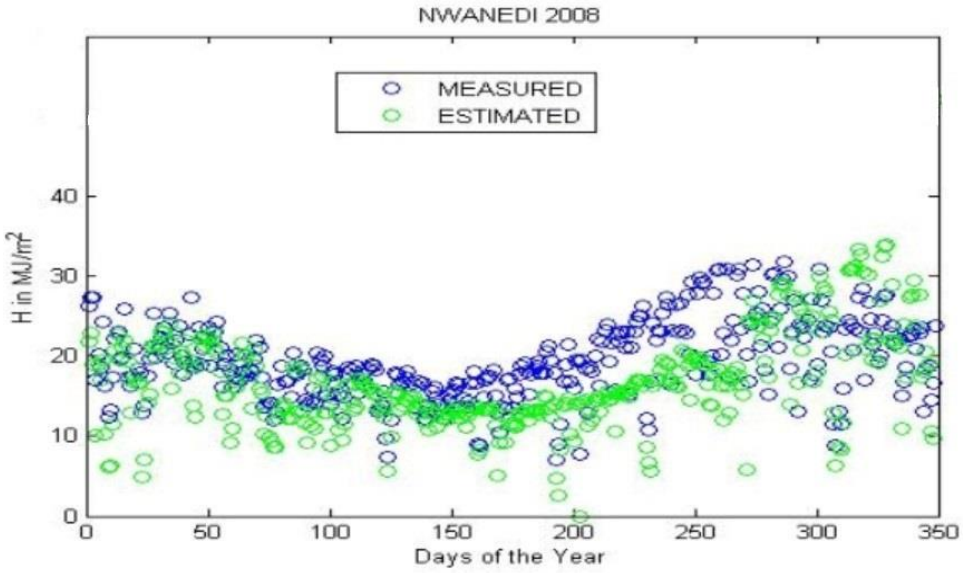

Figure 4.15: Comparisons between the estimated and the measured global solar radiation for Nwanedi (2008).

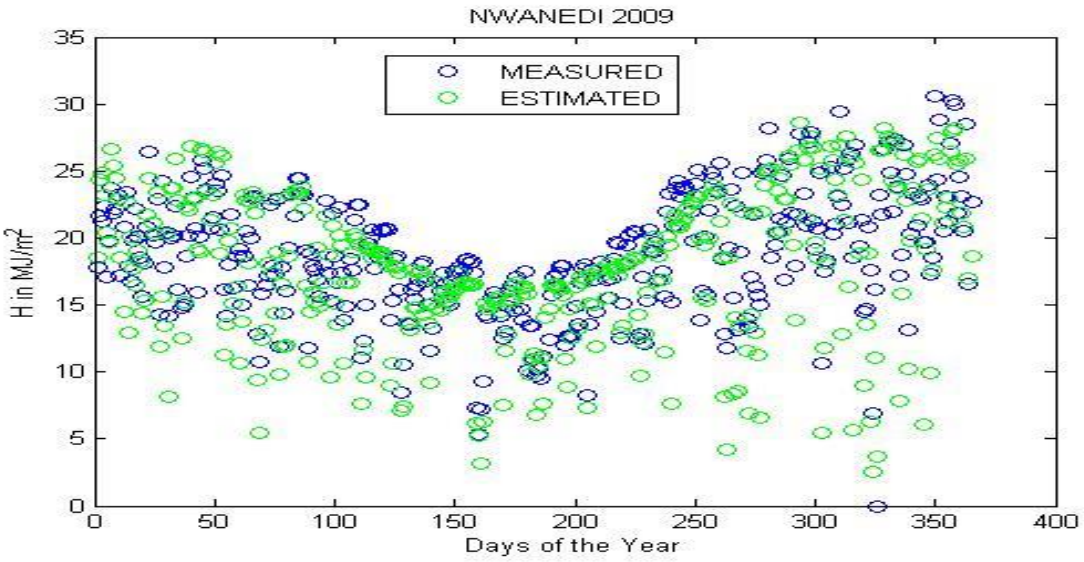

Figure 4.16: Comparisons between the estimated and the measured global solar radiation for Nwanedi station (2009).

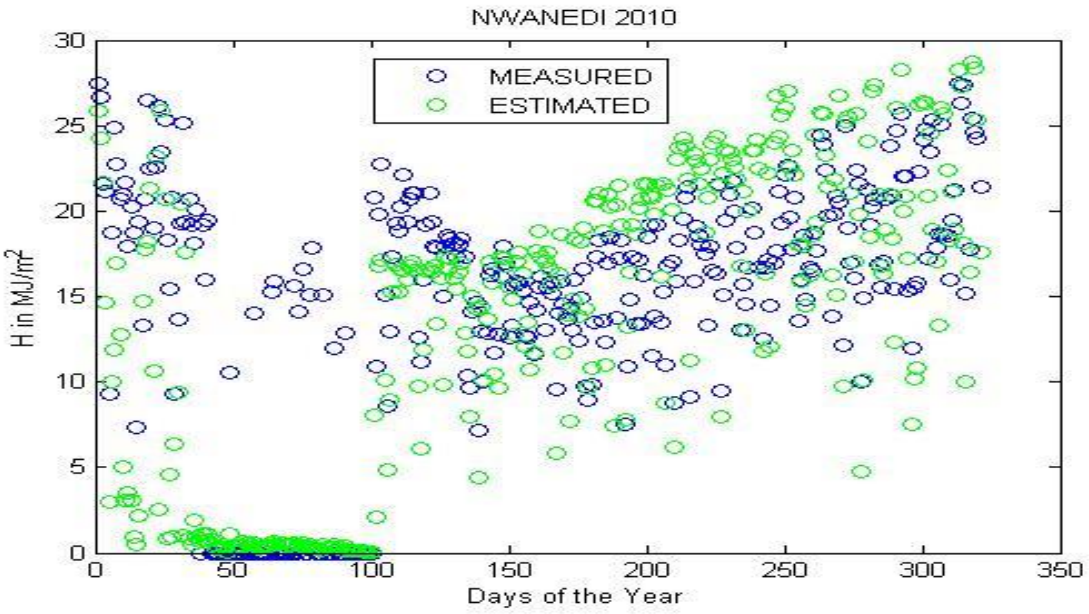

Figure 4.17: Comparisons between estimated and the measured global solar radiation for Nwanedi station (2010).

Table 4.21: Average values for statistical tests.

Year	Station	RMSE	MBE	MPE	R^2
2008	Nwanedi	0,0151	0,0072	0,7227	0,9020
2009	Nwanedi	0,0025	0,0025	0,2520	0,9708
2010	Nwanedi	0,0101	0,0037	0,3701	0,7935

The statistical comparison also highlights that for Nwanedi stations Hargreaves and Samani model can be used to estimate the global solar radiation as shown in Table 4.21. The table shows the obtained statistical values from the comparison between the measured and estimated values of the global solar radiation. It is clear from the table that the values of the *MPE*, *MBE* and *RMSE* values are lower. From Table 4.21. for 2009, RMSE = 0, 0025, MBE = 0, 0025, MPE = 0, 2520 and R^2 = 0, 9708 which is approximately equal to 1 as expected. Hence for the year 2008 – 2010 the value ranges from RMSE= 0, 0025 to 0, 0151, MBE= 0, 0058 to 0, 0080, MPE= 0, 0025 to 0, 7227 and R^2 = 0, 7935 to 0, 9708. This indicates that the model can be also used to estimate the global solar radiation in Nwanedi area.

Table 4.22: Roedtan monthly average global solar radiation for measured and estimated data from 2008 – 2010.

Year	2008		2009		2010	
Months	Measured (MJ/m^2)	Estimated (MJ/m^2)	Measured (MJ/m^2)	Estimated (MJ/m^2)	Measured (MJ/m^2)	Estimated (MJ/m^2)
Jan	16.16	16.30	15.40	18.80	16.13	16.19
Feb	16.73	16.82	16.69	19.75	17.72	16.08
Mar	18.11	24.45	20.02	24.14	17.40	18.76
Apr	17.19	19.91	19.29	15.57	12.52	13.02
May	16.13	26.04	15.46	14.22	15.16	14.04
June	11.63	12.49	11.67	9.28	11.24	12.70
July	11.51	12.27	11.18	9.48	10.51	11.82
Aug	14.73	15.00	13.83	11.65	12.74	13.74
Sep	16.16	16.30	15.40	18.80	16.13	16.19
Oct	16.73	16.82	16.69	19.75	17.72	16.08
Nov	16.10	13.08	16.81	19.60	15.62	17.03
Dec	24.32	22.32	19.04	21.02	22.44	25.34

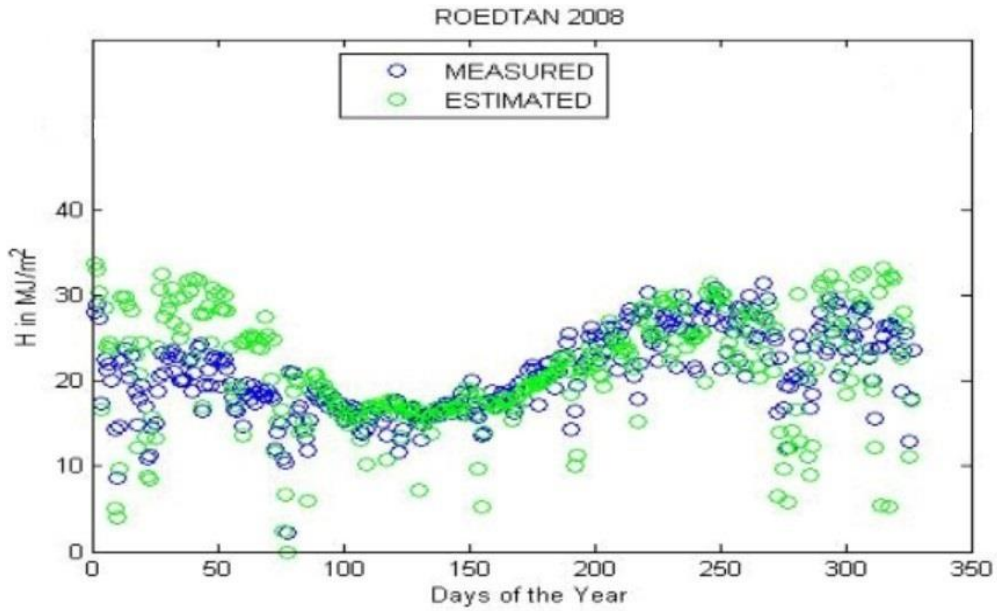

Figure 4.18: Comparisons between the estimated and the measured global solar radiation for Roedtan station (2008).

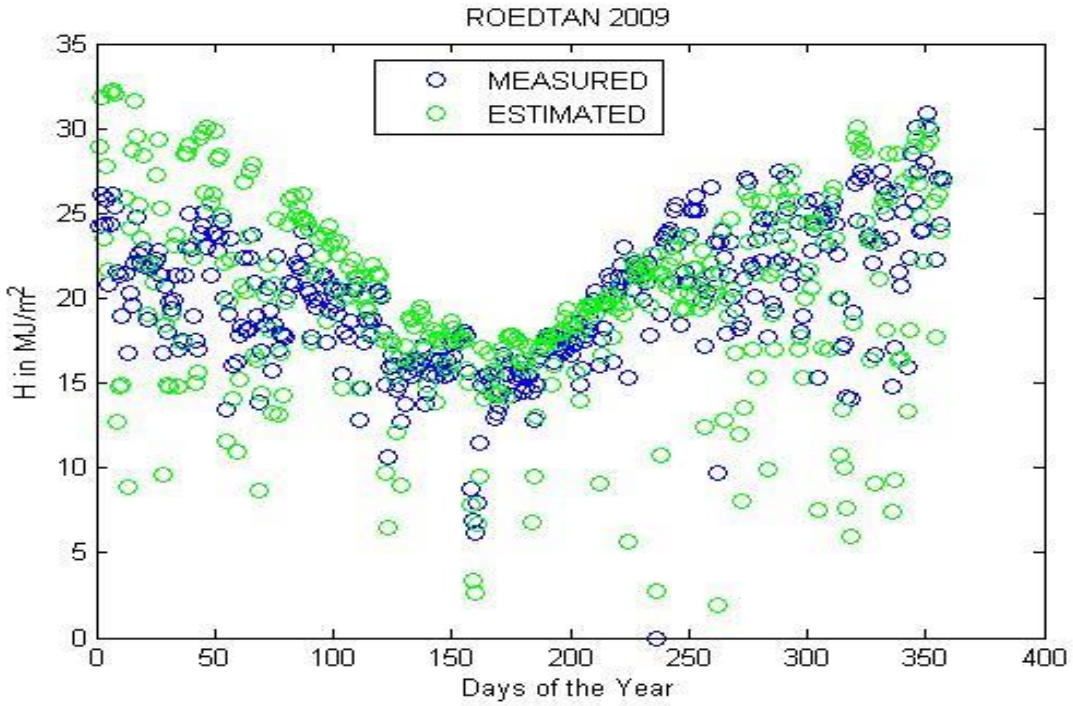

Figure 4.19: Comparisons between the estimated and the measured global solar radiation for Roedtan station (2009).

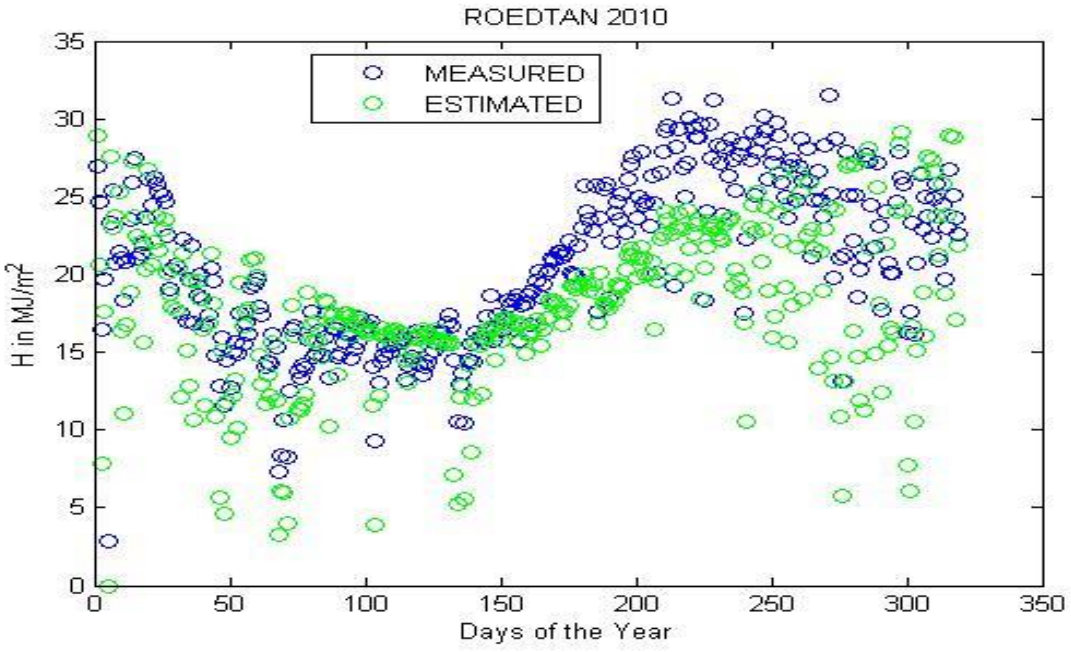

Figure 4.20: Comparisons between the estimated and the measured global solar radiation for Roedtan station (2010).

Table 4.23: Average values for statistical tests.

Year	Station	RMSE	MBE	MPE	R^2
2008	Roedtan	0,0144	-0,0018	-0,1790	0,9515
2009	Roedtan	0,0097	2,2424e-004	0,0224	0,9696
2010	Roedtan	0,0101	-9,2719e-004	0,0927	0,9627

Table 4.22 shows the average monthly values of the estimated and measured global solar radiation. The values follows similar trends to other stations. It can be noted that there is also pact between the measured and estimated global solar radiation values for each year. The maximum values of the global solar radiation are obtained in Summer and the minimum values are obtained in Winter respectively, they range from 9.48 MJ/m^2 to 26.04 MJ/m^2 for the years 2008 – 2010 understudy. Figures 4.18 – 4.19 illustrate the scatter plots of the estimated and measured daily average global solar radiation. It can be observed from the figure that the estimated and measured global solar radiation data is in good pact.

The statistical comparison also indicates that for Roedtan station Hargreaves and Samani model can be used to estimate the global solar radiation as seen in Table 4.23 where it represents the average value for statistical tests for the Mean Percentage Error (*MPE*), Mean biased Error (*MBE*) and Root Mean Square Error (*RMSE*) values are also lower. Observing in Table 4.23 for 2010, RMSE = 0, 0101, MBE = -9,2719e-004, MPE = 0, 0927 and R^2 = 0, 9627 which is approximately equal to 1 as expected for all the years 2008 - 2010.

Table 4.24: Sekgosese monthly average global solar radiation for measured and estimated data from 2008 – 2010.

Year	2008		2009		2010	
Months	Measured (MJ/m^2)	Estimated (MJ/m^2)	Measured (MJ/m^2)	Estimated (MJ/m^2)	Measured (MJ/m^2)	Estimated (MJ/m^2)
Jan	16.48	19.49	17.73	12.44	18.55	21.07
Feb	21.06	24.83	18.04	11.82	18.21	20.54
Mar	17.40	20.05	15.55	10.54	16.84	18.96
Apr	16.28	17.41	14.29	10.57	11.52	12.42
May	12.80	14.04	13.40	10.94	12.16	14.04
June	11.63	12.49	11.67	9.28	11.24	12.70
July	11.51	12.27	11.18	9.48	10.51	11.82
Aug	14.73	15.00	13.83	11.65	12.74	13.74
Sep	16.16	16.30	15.40	18.80	16.13	16.19
Oct	16.73	16.82	16.69	19.75	17.72	16.08
Nov	16.10	13.08	16.81	19.60	15.62	17.03
Dec	18.11	24.45	20.02	24.14	17.40	18.76

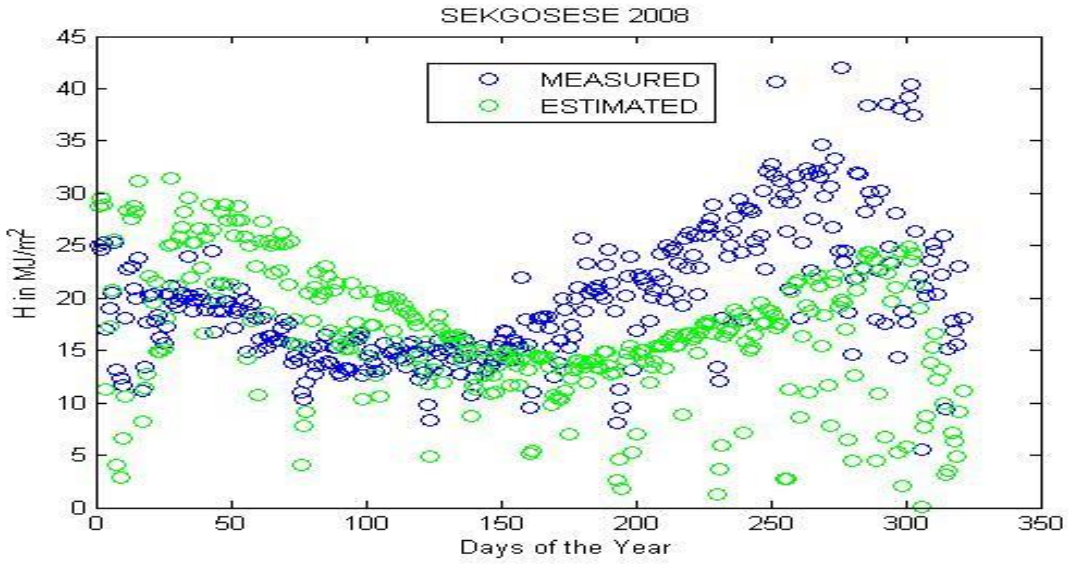

Figure 4.21: Comparisons between the estimated and the measured global solar radiation for Sekgosese station (2008).

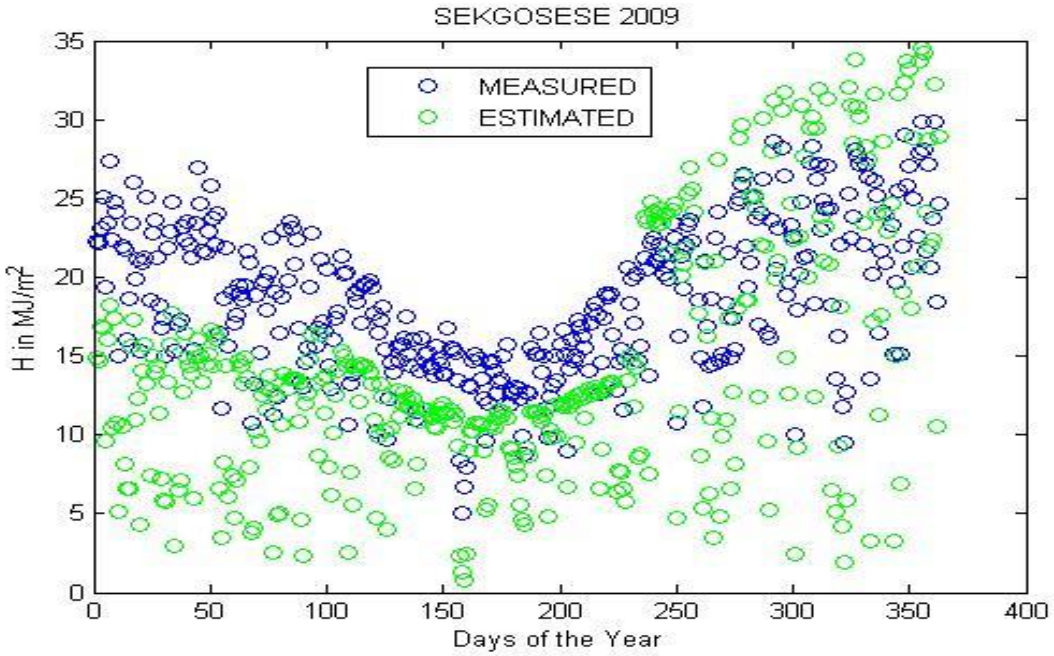

Figure 28: Comparisons between the estimated and the measured global solar radiation for Sekgosese station (2009).

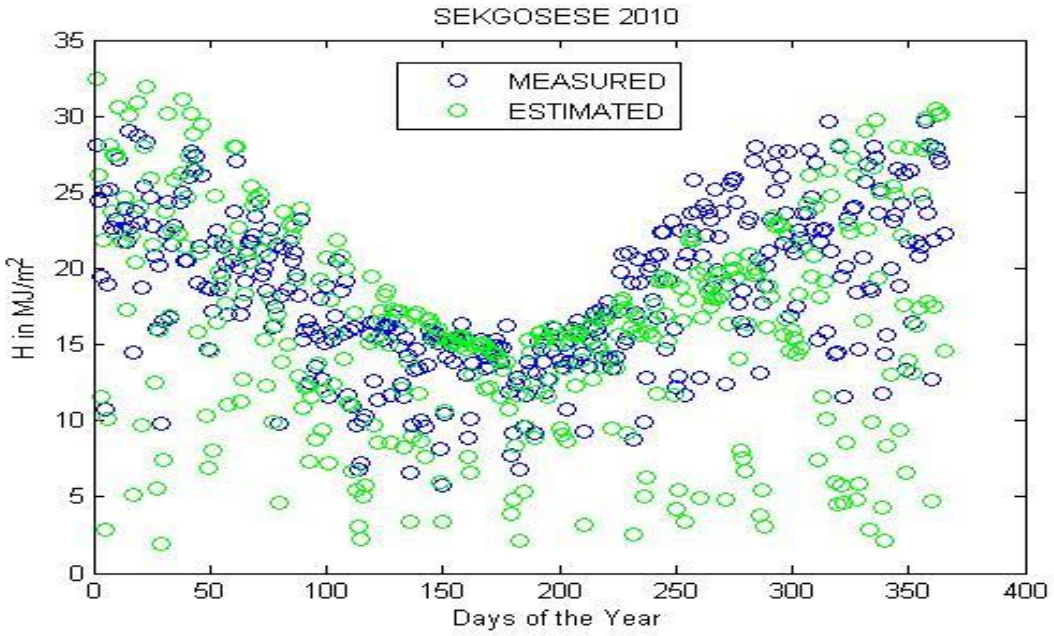

Figure 4.23: Comparisons between the estimated and the measured global solar radiation for Sekgosese station (2010).

Table 4.25: Average values for statistical tests.

Year	Station	RMSE	MBE	MPE	R^2
2008	Sekgosese	0,0248	0,0107	0,0717	0,7656
2009	Sekgosese	0,0169	0,0116	0,1640	0,8179
2010	Sekgosese	0,0122	0,0063	0,6286	0,9244

Table 4.26: Xikundu monthly average global solar radiation for measured and estimated data from 2008 – 2010.

Year	2008		2009		2010	
Months	Measured (MJ/m^2)	Estimated (MJ/m^2)	Measured (MJ/m^2)	Estimated (MJ/m^2)	Measured (MJ/m^2)	Estimated (MJ/m^2)
Jan	16.91	12.54	16.91	16.79	18.66	18.45
Feb	15.87	12.74	12.69	14.75	18.74	19.54
Mar	14.32	14.83	12.64	13.00	17.00	17.62
Apr	13.66	12.76	13.83	16.54	18.64	17.72
May	10.09	6.59	9.25	13.55	10.81	18.83
June	11.94	9.04	16.64	16.69	16.88	18.77
July	17.33	12.71	17.66	16.96	18.54	18.41
Aug	16.59	13.02	7.49	14.19	19.89	17.15
Sep	15.36	13.23	17.81	19.49	19.59	17.58
Oct	14.65	13.32	9.04	13.46	16.90	17.54
Nov	15.62	13.35	14.61	15.59	16.86	12.69
Dec	16.70	26.39	17.20	17.83	10.42	12.68

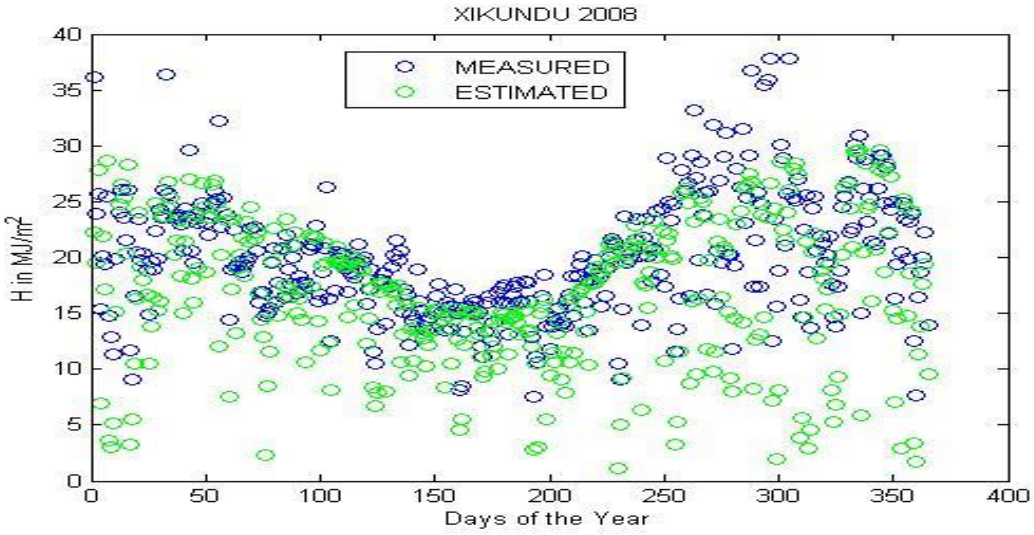

Figure 4.24: Comparisons between estimated and the measured global solar radiation for Xikundu station (2008).

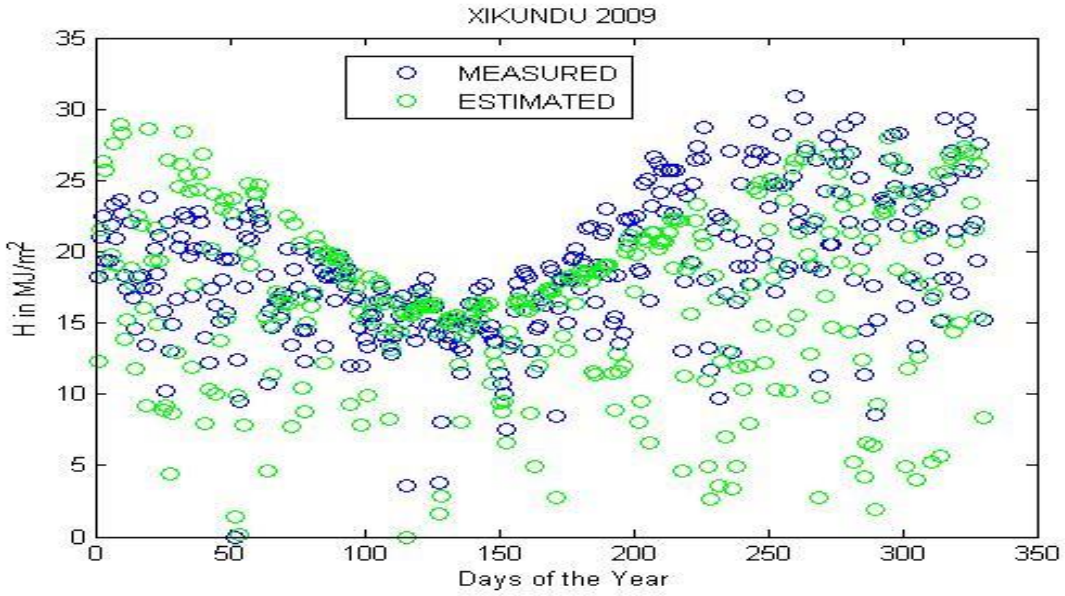

Figure 4.25: Comparisons between the estimated and the measured global solar radiation for Xikundu station (2009).

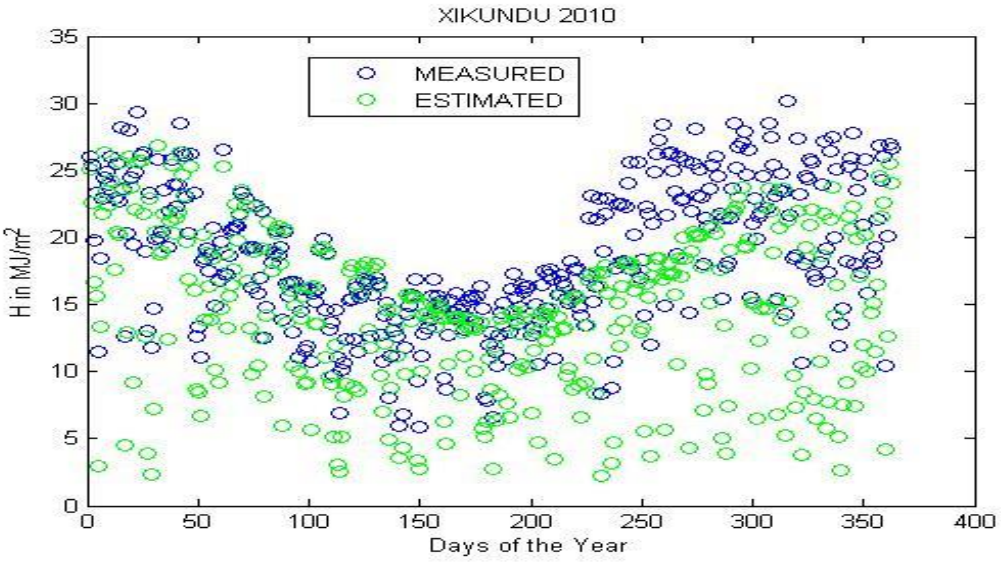

Figure 4.26: Comparisons between the estimated and the measured global solar radiation for Xikundu station (2010).

Table 4.27: Average values for statistical tests.

Year	Station	RMSE	MBE	MPE	R^2
2008	Xikundu	0,0139	0,0083	0,8281	0,9095
2009	Xikundu	0,0130	0,0067	0,6705	0,9339
2010	Xikundu	0,0141	0,0109	1,0949	0,8751

Table 4.28: Average values for H (2008 – 2010) for the stations under study.

Station	2008 (MJ/m^2)	2009 (MJ/m^2)	2010 (MJ/m^2)
Ammondale	20.37	20.59	19.38
Mutale	21.21	24.36	20.30
Nwanedi	26.46	25.12	23.68
Roedtan	19.20	20.19	17.97
Sekgosese	24.23	23.54	20.19
Xikundu	22.55	23.31	20.04

To understand the behavior of the global solar radiation in other areas, Sekgosese and Xikundu the global solar radiation data were also estimated and compared to the measured data. The comparison gives a good indication that Hargreaves and Samani temperature models can be used to estimate the global solar radiation in those areas. As stated before the highest and lowest values of global solar radiation (*H*) are obtained in Summer and Winter respectively. From Table 4.24 and 4.26 it can be observed that the estimated and measured average monthly global solar radiations are comparable for each station. By observing Figures 4.21– 4.23 for Sekgosese and Figures 4.24 – 4.26 for Xikundu, it can be noted that there is a good agreement between the daily average global solar radiations throughout the year.

This is also evident from the lower values obtained for *RMSE, MBE, and MPE*. These statistical values shows that the temperature data can be used to estimate the global solar radiation in these areas. The percentage error obtained between the estimated and observed global solar radiation data is below 10% across all the months of the year for different stations under study. The statistical test for this theoretical model is further demonstrated by the low values of the *RMSE, MBE, MPE,* and R^2 as in Tables 4.25 and 4.27. As these are statistical indicators, their lower values shows that the model can be used to estimate the global solar radiation. This is also evident from the values obtained for R^2 which are closer to unity.

Table 4.28 highlights annualy average global solar radiation data for each station, it can be observed that there is a good coverage of the solar radiation falling under this area. They are suitable for the installation of the renewable energy technologies and solar plants. The Hargreaves and Samani models can be used to estimate the global solar radiation as evidence from the results obtained.

4.5 SUMMARY OF THE RESULTS.

In general, the percentage error obtained between the estimated and observed global solar radiation data is below 10% across all the months of the year for different stations under study. The model shows that it can work under any climatic region provided the region can be classified as inland or coastal based on the observed data in this research. The calculated value of the empirical coefficient obtained agrees well with

the value suggested by Hargreaves and Samani [6]. Thus, the measured temperature data for the area under study can be used to calculate the empirical coefficient K_r. Since the K_r value obtained is equal to the value suggested by Samani, and then it can be used to estimate the global solar radiation. The comparison of the extraterrestrial global solar radiation (H_o), global solar radiation (H) and K_r values are listed on different tables and for the H values in each of the selected stations there is a monthly variation.

The extraterrestrial global solar radiation changes regularly with the season for all selected stations as illustrated in Tables 4.8 - 4.13 for 3 years (2008-2010). For example, Ammondale station receives a minimum of 22.62 MJ/m^2, 22.14 MJ/m^{2,} and 22.16 MJ/m^2 which is the lowest in June which is winter from 2008 – 2010 accordingly and with the highest of 42.74 MJ/m^2, 42.88 MJ/m^2 and 42.87 MJ/m^2 during December and January as shown in Table 4.8 and graphically presented in Figure 4.3, the similar scenario goes to Nwanedi, Roedtan, Sekgosese and Xikundu as seen from the tables and figures above. This can be explained as the consequences of the climatological (weather) variations in the atmosphere. In S.A. during Summer high temperature and rainfall are experienced, and also that time where a high global solar radiation is received compared to Winter. Apart from the seasonal change, the regions under study are based in the rural area of Limpopo province, which also shows that as there is little industrial activity in the areas, hence less pollution and global solar radiation can be received without much reflection.

The difference in the estimated and measured results may be caused by the error occurring during the time of the measurements of the data at that particular station or by the fact that the pyranometers may need regular calibration. The data measured in each of the stations mainly differ due to the sensors used and the methodology used to collect such data [48]. The statistical tests, *RMSE, MBE, MPE,* and R^2 were determined for the entire period of the study in different areas. The statistical observations are illustrated in different tables above. The RMSE, MBE, and MPE values obtained are very low and vary in each station. The R^2 values obtained are close to 1, which illustrates that the values obtained for global solar radiation are in comparison with the measured values.

4.6 CONCLUSION

From this investigation, we noticed that it is more preferable to use the temperature-based model by Hargreaves and Samani to estimate global solar radiation, rather than the models based on sunshine hours. However, all selected weather stations are in the hot interior zone and are having greater availability of temperature data. Our results suggest that the models can produce a reliable idea of the global solar radiation data for the climatic conditions of the stations in the Northern regions of Limpopo Province under study.

The results depicted from the figures above graphically demonstrate that the theoretical model is suitable for making a reasonable estimation of all selected areas and fully authentic in all stations. The validity test for this theoretical model was further shown by the low values of the RMSE = 0, 0144, MBE = 0, 0072, MPE = 0, 7152 and $R^2 \geq 0.9$ for over 80 % of the linear regressions. The estimated global solar radiation from the Hargreaves and Samani model for the stations studied was comparable with the quantified data from the ARC and SAWS.

Therefore the expected reliable set of solar radiation data using the temperature-based model was achieved. The global solar radiation in Limpopo province can be estimated using the temperature-based model developed by Hargreaves and Samani. It can be further deduced that from the measured data and estimated data Limpopo province has high global solar radiation falling and is suitable for the installation of solar plant in the regions indicated above.

4.7 Analysis of the dissertation, challenges, and future work recommendations.

The main objective of the study was to test the application of the temperature based model and to determine the global solar radiation data in the location mentioned above. Hence the specific objectives of the study were to analyze the global solar radiation, temperature, and other meteorological data received from Agricultural Research Council (ARC) and South African Weather Services (SAWS) and hence classify them according to the different climatic conditions for the identified sites, to compute the values of extraterrestrial solar radiation (H_o), global solar radiation (H) and then compare the values obtained through the model and study the applicability of the model on the given location, finally to determine measurement uncertainties and perform statistical analysis. There was a good agreement between the comparisons of each station's monthly average extraterrestrial global solar radiation of 2008 – 2010 as seen in the tables and figures above.

Our estimated and measured global solar radiation data illustrate that in the rural remote area and for the areas under study, and the temperature data which can be used to estimate the global solar radiation. The aim was achieved even though there were minor errors involved due to the use of MATLAB. MATLAB is a multi-paradigm numerical computing environment and propriety programming language, it allows matrix manipulations, plotting of functions and data, and implementations of algorithms. In other areas, there was some missing data for days, weeks, and months which made it less perfect to compute and get the exact results expected, hence the recommendations for future work, it would be to use the data for 10 years so that the difference can be easily spotted, the calibrations of the parameters are done regularly, this type of study be further carried on and new stations be built so that there will be a lot of data in those regions.

REFERENCES

1. Trollip H., Butler A.J., Burton T.C. and Godinho C. (2014). Energy security in South Africa. Cape Town Maps.
2. Muller- Steinhagen H. A. (2003). Vision for Sustainable Electricity Generation.
3. Halacy D.S. (1980). Engineering Fundamentals, New York.
4. Androsky A. (1973). Aerospace Corporation El Segundo, CA, Report No: ATR – 74 – (9470).
5. Spillman C.K., Robbins F.V. and Hines R.H. (1979). Solar Energy for Reduction Fossil Fuel Usage. Farrowing Houses Agricultural Experiment Station Paper No: 79-179A, Kansas State University, Manhattan, KS.
6. Hargreaves G.H. and Samani Z.A. (1985). Applied Engineering in Agriculture. 1(2) pp. 96-99.
7. Abdulrahim A.T., Diso I.S. and El-Jummah A.M. (2011). Continental Journal of Engineering Sciences, 6(3) pp. 30-37.
8. Rühle S. (2016). Tabulated values of the Shockley-Queisser limit for single junction solar cells. Solar Energy. 13 pp. 139.
9. Shockley W., Queisser H. (1961). Detailed balance limit of efficiency of p-n junction solar cells. Journal of Applied Physics. 32 pp. 510.
10. https://energy.gov/eere/sunshot/downloads/research-cell-efficiency-records. National renewable energy laboratory (2012). Research cell efficiency records.
11. Nielsen R. (2005). Social, economic and environmental impacts of renewable energy systems. International Journal of Renewable Energy, 34 pp. 390-396.
12. Sims R.E.H. (2004). Renewable energy: a response to climate change, Solar Energy, 76 (1-3) pp. 9-17.
13. Duffie J.A. and Beckman W.A. (1980). Solar engineering and thermal processes, John Wiley and Sons, New York.
14. Orgill J.F. and Hollands K.G.T. (1977). Correlation equation for hourly diffuse radiation on a horizontal surface. Solar energy, 19(4) pp.357-359.
15. Wild J.P. and McCready L.L. (1950). Observations of the Spectrum of High-Intensity Solar Radiation at Metre Wavelengths. The Apparatus and Spectral Types of Solar Burst Observed. Australian Journal of Chemistry, 3(3) pp.387-398.

16. Dixon A.E. and Leslie J.D. (2013). Solar Energy Conversion: An introductory course.1st Edition, Elsevier.

17. Iqbal M. (2012). An introduction to solar radiation. 1st Edition. Elsevier.

18. Kuciauskas A., Solbrig J., Lee T., Hawkins J., Miller S., Surratt M. and Kent J. (2013). Next-generation satellite meteorology technology unveiled. Bulletin of the American Meteorological Society, 94(12) pp.1824-1825.

19. Fu P. and Rich P. M. (1999). Design and implementation of the Solar Analyst: an ArcView extension for modelling solar radiation at landscape scales. In Proceedings of the Nineteenth Annual ESRI User Conference pp.1-31.

20. Pandey C.K. and Katiyar A.K. (2013). Solar radiation: Models and measurement techniques. Journal of Energy, 1(8) pp. 8. http://dx.doi.org/10.1155/2013/305207.

21. Angstrom A. (1924). Solar and terrestrial radiation. Report to the international commission for solar research on actinometric investigations of solar and atmospheric radiation. Quarterly Journal of the Royal Meteorological Society, 50(210) pp.121-126.

22. King D. L., Kratochvil J. A. and Boyson W. E. (1997). Measuring solar spectral and angle-of-incidence effects on photovoltaic modules and solar irradiance sensors. In Photovoltaic Specialists Conference. Conference Record of the Twenty-Sixth IEEE pp.1113-1116. IEEE.

23. Long C.N. and Ackerman T.P. (2000). Identification of clear skies from broadband pyranometer measurements and calculation of downwelling shortwave cloud effects. Journal of Geophysical Research: Atmospheres, 105(D12) pp.15609-15626.

24. Hansen J.E. and Sir Houghton J. (1998). Global Warming: The Complete Briefing. Journal of Atmospheric Chemistry, 30(3) pp. 409-412.

25. Mousazadeh H., Keyhani A., Javadi A., Mobli H., Abrinia K. and Sharifi A. (2009). A review of principle and Sun-tracking methods for maximizing solar systems output. Renewable and sustainable energy reviews, 13(8) pp.1800-1818.

26. Demain C., Journée M., and Bertrand C. (2013). Evaluation of different models to estimate the global solar radiation on inclined surfaces. Renewable Energy, 50 pp. 710-721.

27. Ertekin C. and Yaldiz O. (2000). Comparison of some existing models for estimating global solar radiation for Antalya (Turkey). Energy Conversion and Management, 41(4) pp. 311-330.

28. Almorox J., Bocco M. and Willington E. (2013). Estimation of daily global solar radiation from measured temperatures at Cañada de Luque, Córdoba, Argentina. Renewable Energy, 60 pp. 382-387.

29. Almorox J., Hontoria C. and Benito M. (2011). Models for obtaining daily global solar radiation with measured air temperature data in Madrid (Spain). Applied Energy, 88(5) pp.1703-1709.

30. John M.E. (2011). Census, governing populations and the girl child. Economic and Political Weekly, pp.10-12.

31. Hargreaves G.H. (1994). Simplified coefficients for estimating monthly solar radiation in North America and Europe. Departmental Paper, Department of Biology and Irrigational Energy, Utah State University, Logan, Utah,1 pp. 235 – 252,

32. Abraha M.G. and Savage M.J. (2008). Comparison of estimates of daily solar radiation from air temperature range for application in crop simulations, Agriculture, Forestry and Meteorology, 148 pp. 401 - 416.

33. Bristow K.L. and Campbell G.S. (1984). On the relationship between incoming solar radiation and daily maximum and minimum temperature. Agriculture, Forestry and Meteorology, 31 pp. 159 - 166.

34. Hunt L.A., Kucharb L and Swanton C.J. (1998). Estimation of solar radiation for use in crop modeling, Agriculture, Forestry and Meteorology, 91 pp. 293 - 300.

35. Yorukoglu M. and Celik A.N. (2006). A critical review on the estimation of daily global solar radiation from sunshine duration, Energy Conversion and Management, 47 pp. 2441-2450.

36. Handcock R.N., Cherkauer K.A., Kay J.E., Gillespie A., Burges S.J. and Booth D.B. (2002). Spatial Variability in Radiant Stream Temperatures Estimated from Thermal Infrared Images. Eos Transactions AGU, 83 pp.47.

37 Hargreaves G.H. and Samani Z.A. (1982). Estimating Solar Radiation and Evapotranspiration. Irrigation and Draining Engineering, 108 pp. 223.

38. Prescott, J.A. (2004). Evaporation from Water Surface in Relation to Solar Radiation. Transactions of the Royal Society of South Australia, 64 pp. 114 - 118.

39. Bristow K.L. and Campbell G.S. (1984). On the relationship between incoming solar radiation and daily maximum and minimum temperature. Agriculture, Forestry and Meteorology, 31 pp. 159 - 166.

40. Michael P. and Kevin V. (2010). Solar radiation. In Encyclopedia of Earth. Eds. <http://www.eoearth.org/article/Solar_radiation>

41. http://www.southafrica.info/travel/advice/climate.htm. Accessed 07 February 2015.

42. Nye S. and David E. (1999). Consuming Power. A Social History of American Energies. The MIT Press: Cambridge, MA, 42 pp. 137 - 138.

43. United States Energy Information Administration (EIA), (2008). Renewables and Alternate Fuels. Solar Photovoltaic Cell/Module Manufacturing Activities.

44. Pathak M.J.M., Sanders P.G. and Pearce J.M. (2014). Optimizing limited solar roof access by energy analysis of solar thermal, photovoltaic, and hybrid photovoltaic thermal systems. Applied Energy, 120 pp. 115 – 124.

45. Ibeh G.F. (2012). Comparison of Artificial Neural Network (ANN) and Angstrom-Prescott models in correlation between sunshine hours and global solar radiation of Uyo city, Nigeria. Archives of Applied Science Research, 4(3) pp.1213 - 1219.

46. United States Energy Information Administration (EIA). (2008). Renewable Energy Consumption and Electricity 2008 Statistics.

47. Anne T. (2008). Solar Revolution. “The Economic Transformation of the Global Energy Industry Major discovery" from MIT primed to unleash solar revolution, 20 pp. 39 – 55.

48. Maluta N.E. and Mulaudzi S.T. (2018). Development of a site-independent mathematical model for the estimation of global solar radiation on Earth’s surface around the globe, International Energy Journal, 18 pp. 181 – 190

49. Simon J.E. (2005). Renewable Energy and Efficiency. Renewable and Sustainable Energy Reviews, 93 Pp. 35-51.

50. Sydenham S. and Thomas R. (2003). Solar Energy and Applied Energy 320 pp. 103 –287.

51. Johnsons L.Y. (2006). The Photovoltaic Effect. Journal of Fluorine Chemistry. Review, 127(3) pp. 303-319.

52. Tiwari G.N. (2012). Energy: Fundamentals, Design, Modelling and Application. Renewable and Sustainable Energy Reviews, 39 pp. 10 –87.

53. McVeigh J.C. (2013). Sunpower. An Introduction to the Applications of Solar Energy Pergamon International Library, 83 pp. 115

54. Wieder S. (1992). An Introduction to Solar Energy for Scientists and Engineers, 32 pp. 103 –127.

55. Weston S. (2012). Global Solar Radiation. Journal of Energy in Southern Africa, 28 (4) pp. 2.78.

56. Liu X., Mei X., Li Y., Wanga Q., Jensen J., Zhang Y. and Porter J. (2009). Evaluation of temperature-based global solar radiation models in China. Agriculture Forestry Meteorology, 149 pp. 1433 - 1446.

57. Iziomon M.G. and Mayer H. (2002). Assessment of some global solar radiation parameterizations. Journal of Atmospheric and Solar-Terrestrial Physics, 64 pp. 1631 - 1643.

58. Tiwari G.N. (2002). Energy. Fundamentals, Design, Modelling and Application. Narosa Publishing House. New Delhi. Accessed 03 September 2009.

59. Sinew D. (2005). Renewable Energy. The Journal of hand surgery, Elsevier. 30(2) pp. 13 –28.

60. Cohen H. (2003). From Core to Corona: Layers of the Sun. www.fuseweb.pppl.gov/CPEP/Chart Page/5 plasmas/Sunlayers.html. Accessed 04 April 2016.

61. Rolando K.V. (2011). Solar Radiation, Scientific Journal of Renewable Energy, 320 pp. 1013 –1287.

62. Excell R.H.B. (2000). The Intensity of Solar Radiation. Renewable energy journal, 3 pp. 10 – 38.

63. Iqbal M. (2003). An Introduction to Solar Radiation. Solar Energy and Applied Energy, 1 pp. 15 – 280.

64. Liou K.N. (1980). Introduction to Atmospheric Radiation. Scientific Journal of Renewable Energy, 100 pp. 103 – 287.

65. Klein S.A. (1977) Predicted and measured global solar radiation in Egypt. Solar Energy, 19 pp. 307 - 311.

66. Angstrom A. (1924). Solar and terrestrial radiation. Report to the international commission for solar research on actinometric investigations of solar and atmospheric radiation. Quarterly journal Research Meteorology Society, 50 pp. 121 - 126.

67. Bashahu M. and Nkundabatware P. (1994). Analysis of daily irradiation data for five sites in Rwanda and one in Senegal. Renewable Energy, 4 pp. 425 - 435.

68. Chidiezie T.C. (2008). Equations for estimating global solar radiation in data sparse regions. Renewable Energy, 33 pp.827-831.

69. Firoz A. and Intikhab U. (2004). Empirical models for the correlation of monthly average daily global solar radiation with hours of sunshine on a horizontal surface at Karachi, Pakistan. Turkish Journal of Physics, 28 pp. 301 - 307.

70. Kustas W.P., Pinker R.T., Schmugge T.J. and Humes K.S. (1994). Daytime net radiation for a semiarid rangeland basin from remotely sensed data. Agriculture Forestry Meteorology, 71 pp.337-357.

71. Mechlouch R.F. and Brahim A.B. (2008). A global solar radiation model for the design of solar energy systems. Asian Journal Science Research, 1 pp. 231 - 238.

72. Muneer T.S. Younes B. and Munawwar S. 2007. Discourses on solar radiation modeling. Renewable Sustainable Energy Revelation, 11pp. 551- 602.

73. Museruka C. and Mutabazi A. (2007). Assessment of global solar radiation over Rwanda. Proceedings of the Clean Electrical Power, 2007. ICCEP '07. International Conference, May 21-23, 2007, IEEE Computer Society Press, 7 pp. 670 - 676.

74. Liu B.Y.H and Jordan R.C. (1960). The interrelationship and characteristic distribution of direct, diffuse and total solar radiation, Solar Energy, 4 pp. 1 - 19.

75. Wehrli C. (1985). Extraterrestrial Solar Spectrum, Physikalisch-Meteorologisches Observatorium + World Radiation Center (PMO/WRC), Publication no. 615.

76. Tshiala F.M., Olwoch J.M. and Engelbrecht F.A. (2011). Analysis of Temperature Trends over Limpopo Province, South Africa, Journal of Geography and Geology, 3(1).

77. Mosase E. and Ahiablame L. (2018). Rainfall and Temperature in the Limpopo River Basin, Southren Africa: means, Variations and Trends from 1979 to 2013, Water, 10, pp. 364 - 379